

AD-A140 057

ANODIC OXIDE FORMATION ON TI-6Al-4V IN CHROMIC ACID FOR
ADHESIVE BONDING(U) VIRGINIA POLYTECHNIC INST AND STATE
UNIV BLACKSBURG A M CHENG ET AL. MAR 84 VPI-E-84-8

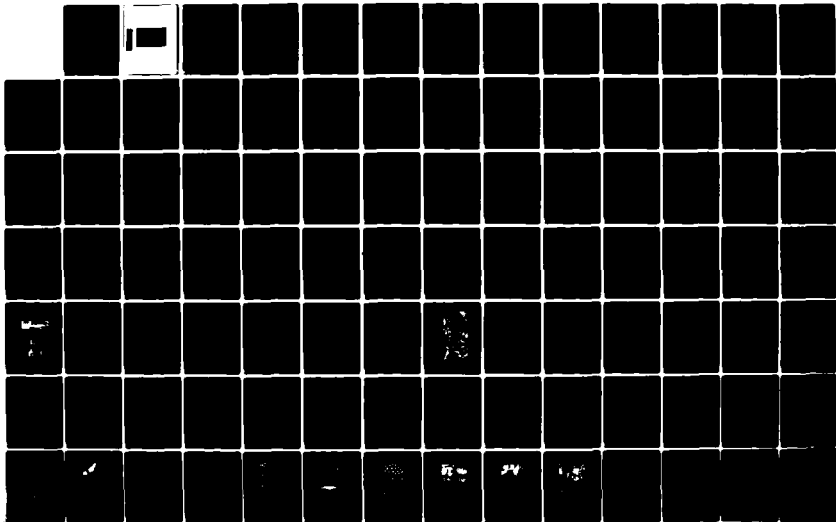
1/2

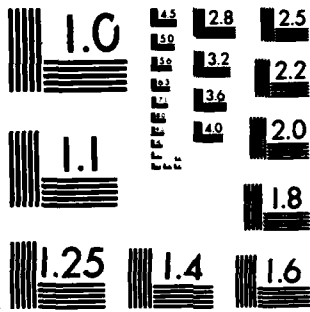
UNCLASSIFIED

N00014-B2-K-0185

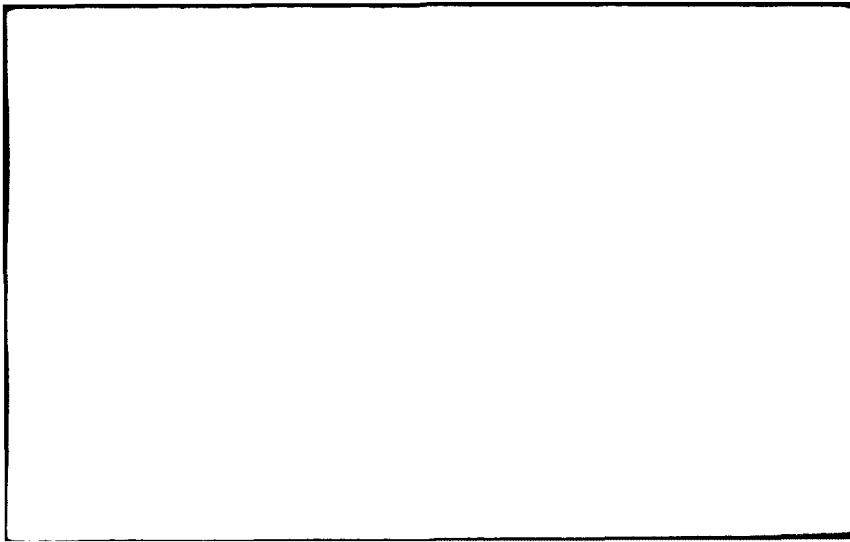
F/G 11/6

NL





MICROCOPY RESOLUTION TEST CHART
NATIONAL BUREAU OF STANDARDS-1963-A



College of Engineering
Virginia Polytechnic Institute and State University
Blacksburg, VA 24061

VPI-E-84-8

March 1984

CATHODIC OXIDE FORMATION ON Ti-6Al-4V
IN CHROMIC ACID FOR ADHESIVE BONDING

Alvin M. Cheng and David W. Dwight

Center for Adhesion Science
and
Departments of Chemical and Materials Engineering
Virginia Polytechnic Institute and State University
Blacksburg, Virginia 24061

Sponsored by:

Office of Naval Research
Grant No. N00014-82-K-0185
800 N. Quincy St.
Arlington, VA 22217

SDTIC
ELECTE
APR 11 1984

A

This document has been approved
for public release and sale; its
distribution is unlimited.

BIBLIOGRAPHIC DATA SHEET	1. Report No.	2.	3. Recipient's Accession No.
4. Title and Subtitle "Anodic Oxide Formation on Ti-6Al-4V in Chromic Acid for Adhesive Bonding"			5. Report Date March 1984
7. Author(s) Alvin Man-tuen Cheng and David W. Dwight			6.
9. Performing Organization Name and Address Center for Adhesion Science and Departments of Chemical Engineering and Materials Engineering, VPI & SU, Blacksburg, VA 24061			8. Performing Organization Rept. No.
12. Sponsoring Organization Name and Address Office of Naval Research 800 N. Quincy St. Arlington, VA 22217			10. Project/Task/Work Unit No.
			11. Contract/Grant No. ONR N00014-82-K-0185
15. Supplementary Notes			13. Type of Report & Period Covered Interim, 9-30-82 to 12-30-83
			14.
16. Abstracts Chromic acid anodization (CAA) of Ti-6Al-4V alloy has been shown to produce desirable oxide for adhesive bonding. The highly porous oxide layer provides mechanical interlocking with the adhesive or the primer forming a much stronger interface. This leads to stronger and more durable bonds than most other surface pretreatments. Since anodization is an electrochemical process, electrochemical methods are used to elucidate the mechanism and kinetics of the oxide formation. From galvanostatic anodization, the preimmersion oxide thickness is calculated to be in the order of 10 Angstroms. Oxygen evolution is dominant at above 10 V. Oxide breakdown or cracking was observed at potentials above 10 V and at current densities above 11 mA/cm ² . Hydrofluoric acid was found to be essential in the initiation and formation of pores desirable for adhesive bonding. Without HF addition, the oxide formed was compact and uniform regardless of anodizing conditions (before breakdown). In the presence of HF, porous oxide was obtained with pore size distribution increasing with temperature and HF concentration.			
17. Key Words and Document Analysis. 17a. Descriptors Anodization; Titanium Alloy; Ti 6-4; Ti-6Al-4V; Adhesive Bonding; Surface Treatment; Porous Oxide; STEM; SEM; ESCA; XPS			
17b. Identifiers/Open-Ended Terms			
17c. COSATI Field Group			
18. Availability Statement Distribution Unlimited		19. Security Class (This Report) UNCLASSIFIED	21. No. of Pages
		20. Security Class (This Page) UNCLASSIFIED	22. Price

Anodic Oxide Formation on Ti-6Al-4V in Chromic Acid for
Adhesive Bonding

(ABSTRACT)

Chromic acid anodization (CAA) of Ti-6Al-4V alloy has been shown to produce desirable oxide for adhesive bonding. The highly porous oxide layer provides mechanical interlocking with the adhesive or the primer forming a much stronger interface. This leads to stronger and more durable bond than most other surface pretreatments. Since anodization is an electrochemical process, electrochemical methods are used to elucidate the mechanism and kinetics of the oxide formation. From galvanostatic anodization, the preimmersion oxide thickness is calculated to be in the order of 10 Angstrom. Oxygen evolution is dominant at above 10 V. Oxide breakdown or cracking was observed at potentials above 10 V and at current density above 11 mA/cm². Hydrofluoric acid was found to be essential in the initiation and formation of pores desirable for adhesive bonding. Without HF addition, the oxide formed was compact and uniform regardless of anodizing conditions (before breakdown). In the presence of HF, porous oxide was obtained with pore size distribution increased with temperature and HF concentration.

ACKNOWLEDGEMENTS

The authors wish to acknowledge the financial support provided by Office of Naval Research, Arlington, VA 22217, through the grant N00014-82-K-0185 for this research project.

Classification Per	
SECRET	<input checked="" type="checkbox"/>
TOP SECRET	<input type="checkbox"/>
CONFIDENTIAL	<input type="checkbox"/>
UNCLASSIFIED	<input type="checkbox"/>
Subject	
Availability Codes	
AC	
AD	
AE	
AF	
AG	
AH	
AI	



TABLE OF CONTENTS

ABSTRACT	ii
ACKNOWLEDGEMENTS	iii

Chapter

	<u>page</u>
I. INTRODUCTION	1
II. THEORIES OF ADHESION	5
Mechanical Adhesion Theory	6
Molecular Theory	7
Weak Boundary Layer	9
Attachment Site Theory	9
III. LITERATURE SURVEY	12
Anodic Oxide Formation and Growth	15
Theory	15
Oxidation of Titanium	20
Mobility of Ions in the Oxide Film	24
Limiting Oxide Thickness and Breakdown	28
Internal Stress	28
Electrolytic and Dielectric Breakdown	30
Oxygen Evolution	30
Oxide Dissolution	31
Formation of Porous Oxide	32
Nature of Oxide on Titanium	35
Optical Properties of Titanium Dioxide Films	36
IV. EXPERIMENTAL	39
Materials	39
Methods	41
Sample Preparation	41
Apparatus	42
Galvanostatic Anodization	46
Potentiostatic Anodization	47
V. RESULTS AND DISCUSSION	49
Galvanostatic Anodization	49
Calculation of Electrokinetic Parameters	57
Potentiostatic Anodization	65

Effect of HF, Time and Temperature on Oxide	
Morphology	69
X-ray Photoelectron Spectroscopy	83
VI. SUMMARY	88
REFERENCE	91
 <u>Appendix</u>	
	<u>page</u>
A.	97
Calculation of Formation Rate and Electrolytic Parameters	97

LIST OF FIGURES

<u>Figure</u>	<u>page</u>
1. Schematic diagram of adhesive joint strength as a function of degree of surface attachment according to the attachment site theory	11
2. Field-assisted hopping model for migration of charged particles in the forward and reverse direction	16
3. Activation energy diagram when the rate-determining step of oxide formation is (a) at the oxide/metal interface and (b) ion migration within the bulk oxide film.	18
4. Dependence of film thickness on forming voltage	23
5. Oxide growth by (a) anion migration and (b) cation migration.	25
6. Oxide growth by joint cation and anion interstitial transport.	26
7. Isometric drawing of phosphoric acid anodized aluminum surface.	33
8. Schematic of anodization apparatus.	43
9. Anodization apparatus. (a) potentiostat and recorder. (b) anodization bath	44
10. Potential vs. time curves at constant CD.	50
11. SEM photomicrographs showing cracked oxide at a pit formed under high CD or above 10 V.	51
12. Potential vs. log I at anodizing time of 20 minutes	54
13. Potential vs. log I at anodizing time of 60 minutes	55

14.	Comparison of an ideal and a typical voltage/time curve	56
15.	$\text{Log}(dE/dt)_I$ vs. $\text{log } I$	58
16.	Unitary formation rate, $(1/I)\{dE/dt\}_I$, vs. $\text{log } I$	60
17.	Potential vs. $\text{log } I$ at constant anodizing times of 3 min., 6 min. and 9 min.	61
18.	E/Q relation at constant I	63
19.	$E/\text{log } I$ relation at constant Q	64
20.	Applied voltage vs. voltage measured against SCE.	66
21.	Current/time relation under constant potential.	67
22.	STEM photomicrographs of anodized Ti-6-4 surfaces. (a) at constant current density $I=1.35 \text{ mA/cm}^2$. (b) at constant $I=1.35 \text{ mA/cm}^2$ until the voltage reached 10 V then switched to constant potential; total anodizing time in both cases is 20 minutes. (50,000X)	70
23.	STEM photomicrographs of CAA Ti-6-4 at 10 V for 2 minutes with HF addition.	71
24.	STEM photomicrographs of CAA Ti-6-4 at 10 V for 20 minutes with HF addition	72
25.	STEM photomicrographs of CAA Ti-6-4 at 10 V for 20 minutes with HF addition (high magnification).	73
26.	STEM photomicrographs of Ti-6-4 surface etched by the phosphate/fluoride treatment	76
27.	STEM photomicrographs of CAA Ti-6-4 at 10 V with current density adjusted by HF ($I=5.47 \text{ mA/cm}^2$) at 54 degree C for 20 minutes. (a) 4,800X (b) 25,000X	77
28.	STEM photomicrographs of CAA Ti-6-4 at 10 V for 20 minutes at 54 degree C with $I=5.47 \text{ mA/cm}^2$ adjusted by HF addition. (a) 100,000X (b) 200,000X	78
29.	SEM photomicrographs of CAA Ti-6-4 at 8 V for 20 minutes. (a) with HF addition (b) without HF (18,000X)	79

30.	SEM photomicrographs of CAA Ti-6-4 at 9 V for 20 minutes. (a) with HF addition (b) without HF (18,000X)	80
31.	SEM photomicrographs of CAA Ti-6-4 at 10 V for 20 minutes. (a) with HF addition (b) without HF (10,000X)	81
32.	SEM photomicrographs of CAA Ti-6-4 at 10 V for 16 minutes. (a) with HF addition (b) without HF (10,000X)	82
33.	Wide and narrow scans XPS spectra of CAA Ti-6-4 surface	85
34.	Model of metal/oxide system	98

LIST OF TABLES

<u>Table</u>	<u>page</u>
1. Classification of metals in order of thermodynamic nobility.	13
2. Interference color vs. oxide thickness for titanium .	37
3. Chemical composition of the Ti-6Al-4V alloy	40
4. XPS peak position of elements on CAA Ti-6-4 surfaces.	87

Chapter I

INTRODUCTION

Titanium and its alloys have received much attention in recent years, particularly in the aerospace industry[1] where high strength, high temperature alloys are needed. Titanium alloys have been used in making aircraft frame, turbine engine parts, pressure vessels, rocket motor cases, etc.. They are characterized by their excellent strength-to-weight ratio, wide range of service temperature, excellent fatigue, crack propagation and corrosion resistance. Of all the titanium alloys, Ti-6Al-4V is by far the most popular[2].

Many applications of Ti-6Al-4V require ways of fastening the parts together. Adhesive bonding offers marked advantages over conventional fastening[3], such as, bolting, riveting or welding. Adhesive bonding eliminates the requirement for drilling holes which serve as stress-risers and the possibility of pitting corrosion around the fasteners. The adhesive joins to the entire bonded area providing a more evenly distributed load. Welding involves the contact of two dissimilar metals which could lead to galvanic corrosion. In most cases, the adhesive is non-conductive and can form an air and moisture-tight seal

around the joint minimizing the possibility of corrosion. Furthermore, in fastening many composite structures, adhesive bonding is the only feasible method as in the case of honeycomb sandwich structures. The overall weight reduction and lower manufacturing cost can lead to substantial savings as well.

There are many factors governing the formation of strong bonding between metals. It is well accepted that adhesive or interfacial failures are indicative of weak joints. Means of strengthening the interphase region so that failure would occur cohesively within the bulk adhesive or adherent is of paramount importance. With that in mind, one of the most important steps in bonding metals is the surface treatment of the metal prior to bonding.

The surface treatment usually serves several purposes. It removes grease, oil contaminants, loose oxides or debris left from machining of the metal. More importantly, it creates a "customized" surface layer which enhances bondability.

There are different surface treatments available for different metals. Generally, they fall into one of the three categories: mechanical, chemical, and electrochemical. Mechanical treatments involve roughening the metal surface by abrasion, such as sanding or grit blasting. This method

removes potential weak boundary layers and creates macro-roughness on the surface. Provided that the debris from the abrasion is completely removed and the adhesive or primer wets the metal surface properly, adhesion is generally improved by this treatment. Chemical treatments can create a stable and cohesively strong metal oxide on the surface. Electrochemical treatment usually is called anodization. It is the anodic oxidation of the metal in an oxidizing electrolyte under an applied electrical potential. Anodization is limited to metals which have self-healing oxide layers. The metal has to be able to form an adherent and insulating film as soon as it is exposed to an oxidizing medium. The film formed will hinder further oxidation reactions. Aluminum and titanium are two of the common metals which can be anodized to create an oxide layer with desirable thickness, morphology and topography for adhesive bonding.

The purpose of this report is to study the chromic acid anodization process with a fundamental approach. Since the anodization process itself is electrochemical in nature, the initiation of the oxide, the kinetics and mechanism of the oxide formation which eventually lead to the final bonding surface are all governed by the electrokinetic parameters. Potentiostatic and galvanostatic experiments are carried out

to elucidate the role of current density and potential in the oxide formation as well as other variables pertinent to the understanding of the anodizing process. Surface techniques such as high resolution scanning electron microscopy (STEM and SEM) and photoelectron spectroscopy (XPS or ESCA) are used to characterize the surfaces produced. It is hoped that the information derived from this study can lead to better understanding in chromic acid anodization(CAA), and improvements can be made to optimize the process to achieve better and consistent adhesive joint strength and durability.

Chapter II

THEORIES OF ADHESION

In spite of the advantages and popularity in using adhesives for bonding primary and secondary structures in many industries, there is no unified theory on adhesion or adhesive joints, nor is there unanimity on even the fundamental notion of what causes materials to stick together. There have been a number of theories proposed in the past. Most theories attempt to explain a particular aspect of the adhesion mechanism as applied to a particular set of experimental conditions. In reality, the adhesive joint strength is probably dependent on a combination of physical and chemical contributions in a rather complicated manner. Too often, an adhesive joint is considered to be composed of only the adherends and adhesive, and the adherend/adhesive interface is considered to be a well defined boundary. In reality, as pointed out by Sharpe[83], the boundary may be more accurately be described as an "interphase" with some finite thickness. For example, in bonding polymers, inter-diffusion of polymer molecules across the interface would create a new phase with properties quite different from the original bonding surfaces or the bulk materials. Similarly, in bonding

metals with porous oxides, the penetration of the adhesive into the oxide pores essentially creates a new phase with no distinct boundary. Perhaps the lack of understanding of this "interphase" in adhesive bonding and the lack of quantitative approach to the problems have been the source of much disagreement and confusion among workers in the adhesion area. Nevertheless, there are three general theories of adhesion, namely, the mechanical theory, the molecular theory, and the "weak boundary layer" theory proposed by Bikerman[4].

2.1 MECHANICAL ADHESION THEORY

The mechanical adhesion theory is based on the fact that surface roughness or porosity increases true surface area for bonding, promotes wetting and spreading and provides mechanical anchoring sites. Most important of all, surface roughness or porosity provides mechanical interlocking between metal oxide and adhesive. In the case of polyethylene bonded to anodized aluminum adherends[21-23], mechanical interlocking accounts for strong adhesion. Arrowsmith[24] also reported that peel strength on copper and nickel foils bonded with an epoxy adhesive is directly related to the surface topography of the metal surface.

2.2 MOLECULAR THEORY

The molecular theory includes the chemical, diffusion, electrostatic, and acid-base contributions to adhesion. The chemical reaction theory attributes the strength of an adhesive joint to the formation of primary valence bonds at the interface of the adhering materials. This is usually accomplished by using an adhesion-promoting primer which has chemically active groups to react with the metal(oxide) surface. The use of silane coupling agents as adhesion promoters is well established[5-8]. DeLollis[9] and Zisman[10] pointed out that chemical bonding, such as created by using silanes, not only can increase initial bond strength, it also offers better retention of adhesion in severe environments. Brenmen, et al.[11] and Lerchenthal, et al.[12] reported that higher bond strength can be achieved by mechanochemical creation of free radicals on the primer surface by mechanical abrasion with emery paper just prior to bonding. The free radicals are believed to cause chemical bonding at the interface.

The diffusion theory[13] maintains that surface contact at the interface alone is not sufficient for good bonding. Also required is that the molecules of the bonding surfaces be able to diffuse across the interface. This theory is undoubtedly important in bonding polymers. However, it cannot

be applied to bonding metals or glass since diffusion in those cases is not possible at the usual bonding temperature.

The contribution of electrostatic forces to adhesion was suggested by Deryagin, et.al.[14] and Skinner and co-workers[15,16]. According to this theory, the strength of an adhesive joint is dependent on an electrical double layer formed at the adhesive-adherend interface. As detachment occurs, energy is expended in separating the charged surfaces. Electrical discharge is sometimes observed with rupture of adhesive bonds. However, there is no direct evidence that the charge exists at the original interface which was formed by two electrically neutral surfaces.

Fowkes and co-workers[17,18] have shown that electron donor-acceptor interaction at the adhesive-adherend interface is an important adhesion mechanism. Adhesion between dissimilar materials is a result of two intermolecular phenomena: London dispersion forces and acid-base interactions which include hydrogen bonding. Therefore, adhesion of polymers to metal surfaces can be enhanced by matching an acidic oxide surface with a basic polymer or vice versa[19]. The acidity of metal oxide surfaces can be measured experimentally as shown by Mason, Siriwardane and Wightman[20].

2.3 WEAK BOUNDARY LAYER

According to the molecular theory, the strength of an adhesive joint is determined by the magnitude of the interfacial forces (valence, Van der Waal, electrostatic, electron donor-acceptor, etc.). According to the "weak boundary layer" theory[4]. The joint strength is determined only by the cohesive strength of the weakest element in the joint. Failure is believed to occur always cohesively: in the adhesive, adherend, or both, or in some weak boundary layer (WBL). Bikerman reasoned that the probability of a crack initiated and propagated exactly along the interface is extremely slim. Therefore, as long as the surface is properly wetted, there is no need to be concerned with surface forces.

2.4 ATTACHMENT SITE THEORY

The "attachment site theory" proposed by Lewis and Natarajan[25] attempted to incorporate the existing theories to describe the structural properties of adhesives joints and degradation mechanism under adverse environments. The strength of an adhesive joint is considered to be dependent on the boundary layer at the adherent-adhesive interface. This boundary layer consists of mechanically effective sites of either chemical or physical nature. These "attachment

sites" are believed to be of macroscopic dimension. Furthermore, according to this model, when the adhesive joint is exposed to adverse environments, the strength of the adhesive joint is deteriorated through depletion of the number of "attachment sites." When the number of attachment sites is depleted below a threshold point (formation of a weak boundary layer), a change from cohesive to interfacial failure may occur and causes a dramatic decrease in bond strength (Figure 1).

Baun[26] studied the bond strength of evaporated gold and a commercial adhesive on Ti-6Al-4V substrate prepared by different chemical etch times. Bond strength was also measured for specimens exposed to steam. Baun found that the results from dry and steam-exposed specimens were in excellent agreement with the "attachment site theory." Dry bond strength increased slowly with etch time, presumably increasing the number of attachment sites, until it passed the threshold point with sudden increase in bond strength. Beyond the threshold region is the cohesive plateau where failure is mixed or cohesive, and no further change in bond strength is observed with longer etch time. When bonded specimens with etch time above the cohesive plateau were exposed to steam, the reverse path was observed with steam exposure time.

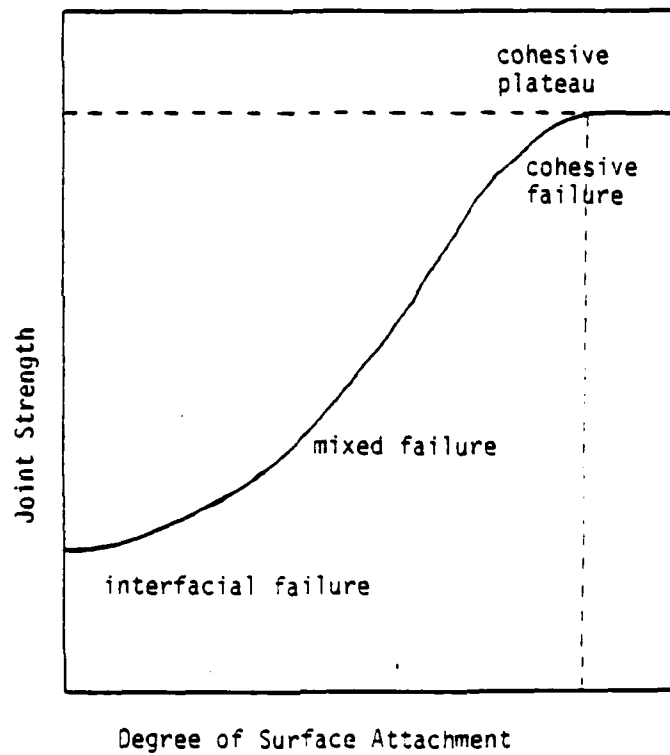


Figure 1: Schematic diagram of adhesive joint strength as a function of degree of surface attachment according to the attachment site theory(25).

Chapter III
LITERATURE SURVEY

Titanium accounts for about 0.6% of the earth's crust. However, metallic titanium was difficult to obtain from its most abundant natural occurrence-- ilmenite (FeTiO_3) and rutile (TiO_2). The common method of reduction by carbon is not possible because titanium forms a very stable carbide. Hence, high-purity titanium was not available commercially until the adoption of the Kroll process in 1949. During this process, ilmenite and rutile are converted to TiCl_4 before finally being reduced to metallic titanium by magnesium[27].

Although titanium is known to be immune to most corrosive and oxidizing environments, it is, in fact, rated as highly reactive in the thermodynamic series[28](Table 1). Its noble behavior is attributed to the natural oxide formed on its surface. The stable, adherent, compact and insulating oxide film essentially halts further reaction with the metal by separating the reactants. The activation energy required for ionic transport across the film is in the order $40kT$ or higher[29]. Under ordinary temperature, thermal energy is insufficient to cause ion migration and oxide thickening. Substantial thickening of the oxide can only be achieved by

TABLE 1

Classification of metals in order of thermodynamic nobility [28].

A		B	
(Immunity)		(Immunity and passivation)	
<u>Noble metals</u>			
1	Gold	Rhodium	1
2	Iridium	Niobium	2
3	Platinum	Tantalum	3
4	Rhodium	Gold	4
5	Ruthenium	Iridium	5
6	Palladium	Platinum	6
7	Mercury	Titanium	7
8	Silver	Palladium	8
9	Osmium	Ruthenium	9
10	Selenium	Osmium	10
11	Tellurium	Mercury	11
12	Polonium	Gallium	12
13	Copper	Zirconium	13
14	Technetium	Silver	14
15	Bismuth	Tin	15
16	Antimony	Copper	16
17	Arsenic	Hafnium	17
18	(Carbon)	Beryllium	18
19	Lead	Aluminium	19
20	Rhenium	Indium	20
21	(Nickel)	Chromium	21
22	(Cobalt)	Selenium	22
23	Thallium	Technetium	23
24	Cadmium	Tellurium	24
25	Iron	Bismuth	25
26	Tin	Polonium	26
27	Molybdenum	Tungsten	27
28	Tungsten	Iron	28
29	Germanium	(Nickel)	29
30	Indium	(Cobalt)	30
31	Gallium	Antimony	31
32	Zinc	Arsenic	32
33	Niobium	(Carbon)	33
34	Tantalum	Lead	34
35	Chromium	Rhenium	35
36	Vanadium	Cadmium	36
37	Manganese	Zinc	37
38	Zirconium	Molybdenum	38
39	Aluminium	Germanium	39
40	Hafnium	Vanadium	40
41	Titanium	Magnesium	41
42	Beryllium	Thallium	42
43	Magnesium	Manganese	43
<u>Non-noble metals</u>			

an applied electric field in an electrolyte as in anodization.

The oxide films on titanium are important in a number of applications other than adhesive bonding. In fact, most literature work reported on the anodic oxidation of titanium is concerned with its insulating or semiconducting properties. Most notably, titanium is highly corrosion resistant in acid or alkaline environments. This passivity is believed to be due to the stable tetravalent TiO_2 [30]. n-type TiO_2 also found application as semiconducting electrode in photoelectrochemical processes [31]. The rutile form of TiO_2 having high dielectric constant is a candidate for use in electrolytic capacitors as well [32].

The anodic behavior of Ti and its alloys is very similar to that of the "valve metals". The original classification of "valve" metal stresses the rectifying characteristic of the oxide-covered metal electrode allowing only cathodic current. A more general characteristic of valve metal as a group is their tendency to form a protective, high-resistance oxide film to the exclusion of all other electrode processes on anodic polarization. Typical valve metals are Ta, Al, Nb, and W. Other metals such as Ti, Si, Mg, Be, Ge and Sn are sometimes classified as valve metals because they behave as an ideal valve metal to a great

extent in certain situations. Therefore the anodic oxidation of other "valve" metals are included in this survey along with Ti and its alloys.

3.1 ANODIC OXIDE FORMATION AND GROWTH

3.1.1 Theory

The early studies of electrokinetics by Guntherschulze and Betz[33] in the 1930's indicated that the ionic current density (I) corresponding to the thickening of oxide films is roughly an exponential function of the field strength (H) as shown in the following equation:

$$I = A \exp(BH) \quad (1)$$

where A and B are constants, and H is the potential drop across the oxide film divided by the film thickness. The form of equation (1) suggests that the field (H) changes the energy barrier of the rate-determining step for ionic current transport. as the ions migrate through the anodic film. In other words, the field lowers the activation energy of the ratelimiting step in the growth of the oxide.

Verwey[34] was the first to propose the field-assisted hopping model (Figure 2) as an explanation for the non-linear dependence of current on voltage observed in anodization experiments.

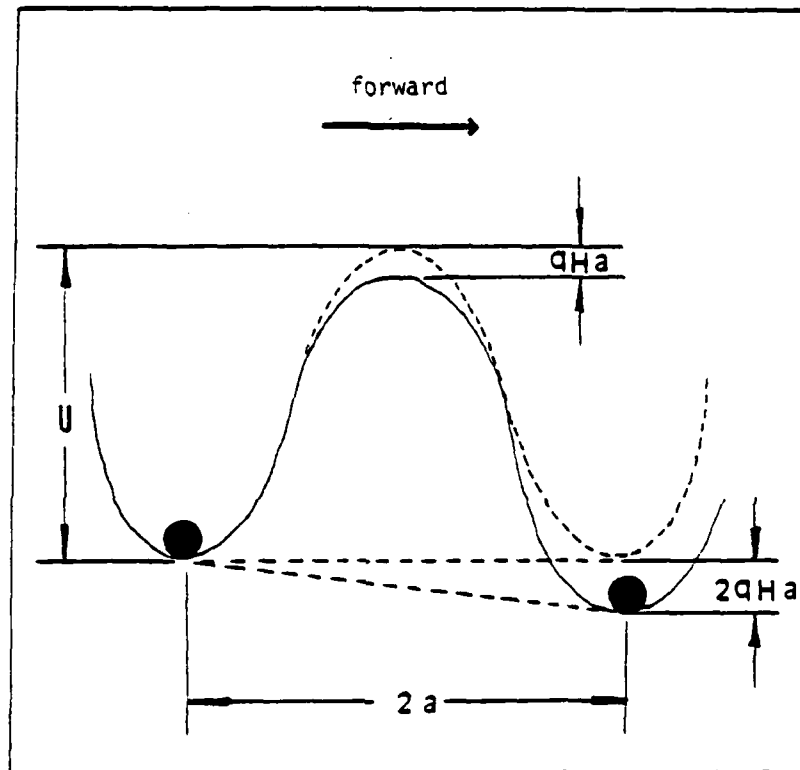


Figure 2: Field-assisted hopping model for migration of charged particles in the forward and reverse direction. Dashed curve represents potential barrier in zero applied field. Solid curve represents the net potential energy barrier with a forward electric field. (Taken from [89])

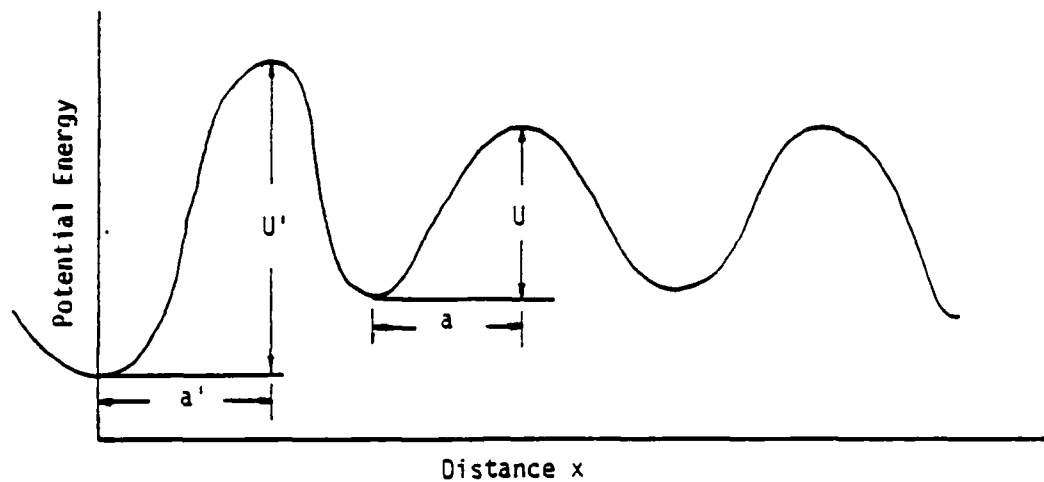
The dashed lines in Figure 2 represents the barrier at zero field, whereas the solid lines represents the field-modified barrier. An electric field, H , lowers the barrier, U , for charged-particle motion in the forward direction and raises it in the reverse by an amount qHa , where q =charge on the ion and a =activation distance.

According to this model, and assuming the reverse current is negligible, the current-field relationship now becomes,

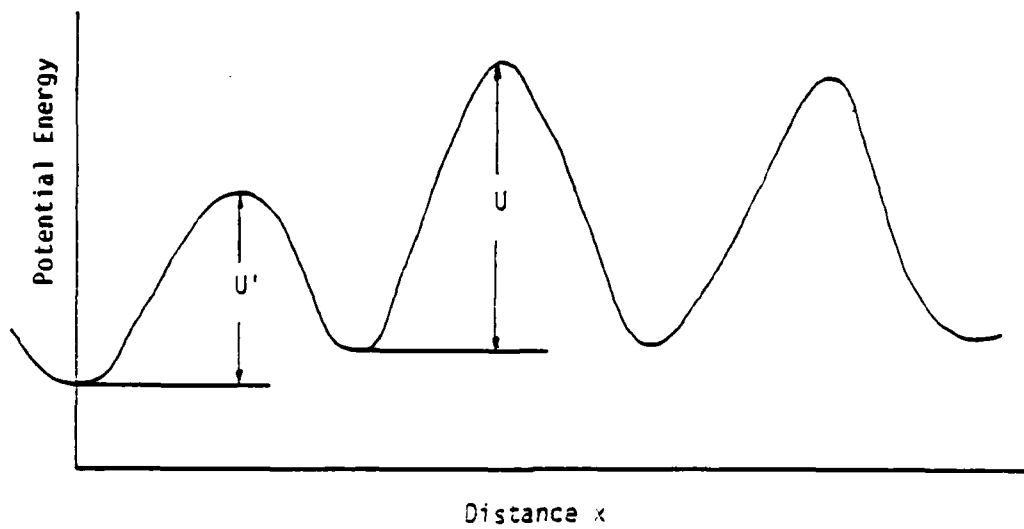
$$I = 2anv \exp\{-((U-qHa)/kT)\} \quad (2)$$

where n =the number of mobile ions per unit volume, v =vibrational frequency, k =Boltzmann's constant, and T =absolute temperature. According to Verwey, the migration of ions within the oxide film is the rate-determining step in the oxide growth (Fig. 3b). He did not consider the effects of the interfaces.

The metal/oxide interface was taken into account by Mott[35] and Cabrera and Mott[36]. They focused on the fact that the entrance activation barrier U' for the transformation : METAL---> ION + ELECTRON, may be greater than the activation barrier U for ion migration through the film itself (Fig.3a). In this case, the rate-determining step lies in the metal/oxide interface. The current-field relationship is similar to the Verwey case except the term



(a)



(b)

Figure 3: Activation energy diagram when the rate-determining step of oxide formation is (a) at the oxide/metal interface and (b) ion migration within the bulk oxide film.

$2an$ is replaced by n' which is the areal concentration of metal ion at the interface.

$$I = n'v' \exp\{-\{(U' - qHa')/kT\} \quad (3)$$

where the prime(') denotes the interface. According to the Mott and Cabrera model, once the metal atom becomes a charged species and jumps across the interface to the oxide lattice, the ion would be pulled across the film immediately under the applied field.

Vermilyea[37] obtained kinetics data on the oxide growth on tantalum using dilute aqueous electrolytes at various temperatures. He concluded from his data, collected by potentiostatic and galvanostatic measurements, that the Mott and Cabrera rate equation must be modified in order to describe the oxide formation on tantalum. An empirical rate equation in the form of:

$$I = P \exp\{-\{(U/kT) - QH\} \quad (4)$$

was suggested where P and Q are constants. However, no mechanism which give rise to the above equation was offered.

In 1954, Dewald[38] incorporated the two possibilities of rate limitation--at the anodic film/metal interface and within the bulk of the oxide--into a single formalism which also takes into account of the effect of space charge within

the film. Dewald's theory, which is based on Mott and Cabrera's rate equation, was able to account for the discrepancy observed by Vermilyea[37] between theory and data on tantalum. The Verwey model and Mott and Cabrera model turn out to be the limiting cases for Dewald's theory. For low-field and thin film cases, the effect of space charge is small, and the contribution of the interface may be dominant(Mott and Cabrera). However, as the film thickness increases, the increasingly large number of barriers, U , would eventually predominate over the barrier U' at the interface even though U' might have been larger at the early stage of film growth. Verwey's model would be valid in this case.

3.1.2 Oxidation of Titanium

Hall and Hackerman[39] measured the anodic charging curves of titanium in neutral 0.5M NaCl solution. The initial rise in potential observed during the constant current density polarization was attributed to the chemisorption of oxygen and charging of the electric double-layer at the oxide/solution interface. The oxide breakdown potential occurs at 10 volts with reference to the saturated calomel electrode(S.C.E.) at which oxygen evolution became visible and pitting was observed. Johansen, Adams and Van

Rysselberghe[40] reported the formation rates of anodic oxide films on Ti and other valve metals in air-saturated ammonium borate solution under galvanostatic condition. Electrolytic parameters, A and B were calculated from the unitary formation rates as a function of metal purity and degree of cold-work.

Sibert[41] reported the effects of various formation parameters, such as, the nature and concentration of the electrolyte, forming voltage, current density and temperature on the properties of the oxide film on commercially pure Ti. In general, two types of films were found. Electrolytes with low solubility for the oxide produced thin translucent films with poor electrical and insulating property. Electrolytes with at least partial solubility for the oxide produced thick, highly insulating and porous films. These observations were made from film resistance and capacity-loss measurements.

There is little doubt that the thickness of the anodic film depends on the voltage which is the driving force for the oxide growth. Theoretically, anodizing under a constant voltage, below that of the oxygen evolution and breakdown voltage, the film could grow to be infinitely thick. However, in reality, as the film thickens, the field (H) across the film decreases rapidly. The ionic current, which

is an exponential function of the field as suggested by Guntherschulze and Betz[33], becomes virtually zero at some finite film thickness and film growth ceases.

Most authors assume a linear relation between final voltage and film thickness[37,41] as shown in Figure 4. As a result, the apparent growth rate is often expressed in units of Angstrom per volt. The reported apparent growth rate ranges from 18[42] to 22[43] and 23.8 Angstrom/V[44] for pure Ti. For Ti alloys, the growth rate may be somewhat lower[45].

According to some authors, the first step in anodic oxidation of titanium might involve the formation of an adsorbed layer of oxygen, or some oxygenated species[39]. Ammar and Kamal[46] observed in anodizing Ti in acid solutions that the open-circuit potential for Ti in H_3PO_4 and HNO_3 decreases with time rather than increasing as in other acids. They concluded that this behavior is due to oxidation of Ti surface rather than the chemisorption of oxygen. Aladjem, Aucouturier and Lacombe[47] reported that passivity may be repeatedly lost and acquired by switching off and on the polarizing current even after the built-up of the anodic film. This result seems to support the mechanism that an adsorbed layer either precedes or accompanies the charging of the electric double-layer at the oxide/solution

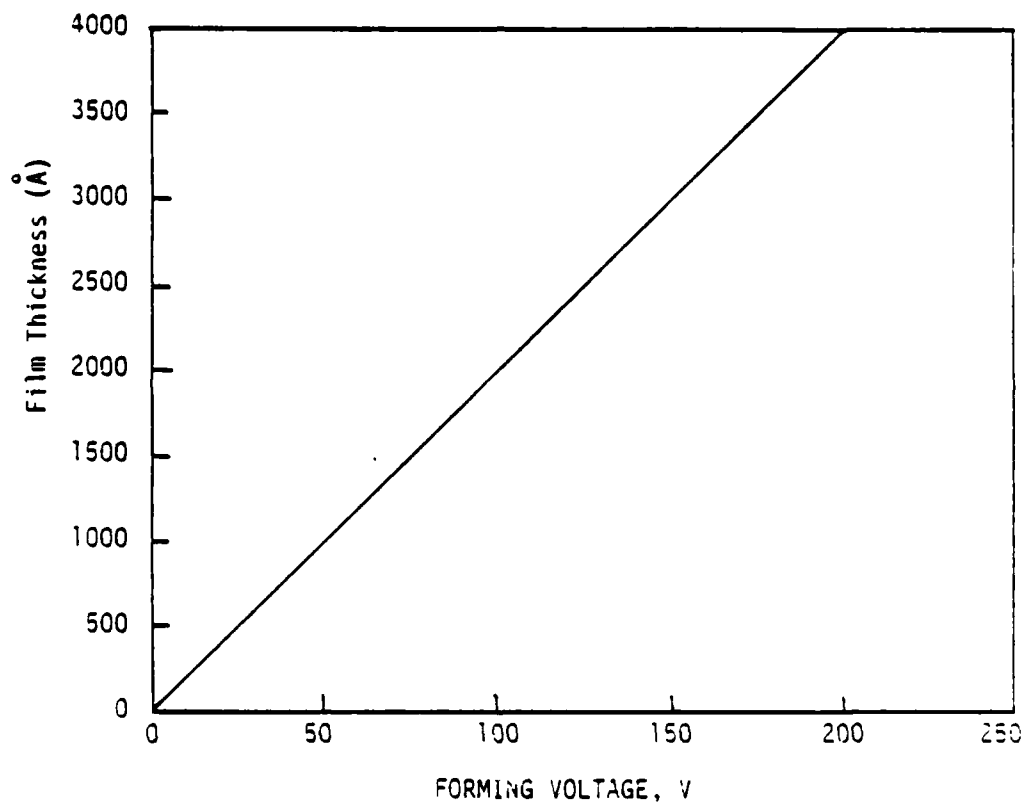


Figure 4: Dependence of film thickness on forming voltage [41].

interface. While there is little doubt that passivity primarily results from either an oxide film or adsorption, the presence of an oxidizing species is essential for the oxidation[48].

3.1.3 Mobility of Ions in the Oxide Film

The growth of the anodic film relies on the transport of ions through the film. If only oxygen ions are mobile, they would migrate through the film under the electric field from the oxide/solution interface and form fresh oxide at the metal/oxide boundary (Figure 5a). By the same token, if only metal ions are mobile, they would migrate and form fresh layers of oxide at the oxide/solution interface (Figure 5b). If both ions are mobile, oxide may be produced simultaneously at both interfaces or, ion by ion, within the body of the existing oxide (Fig 6).

To determine which type of ion is mobile, one only need to determine where new layers are located in the oxide film. This is usually done by building a marker layer which is different from the bulk oxide and determine where the marker layer is in the film by successively dissolving layers of oxide in hydrofluoric acid. The dissolution rate of the oxide in HF would have to be measured beforehand. Lewis and Plumb[49] used radioactive S^{35} as marker in anodizing

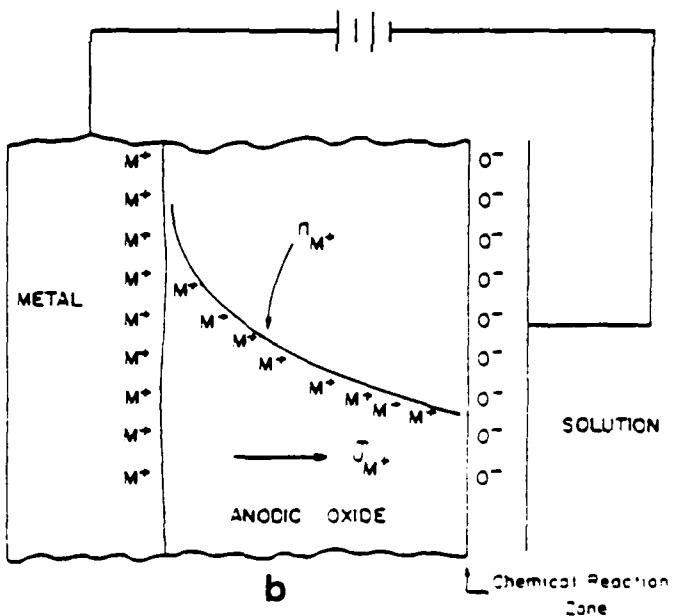
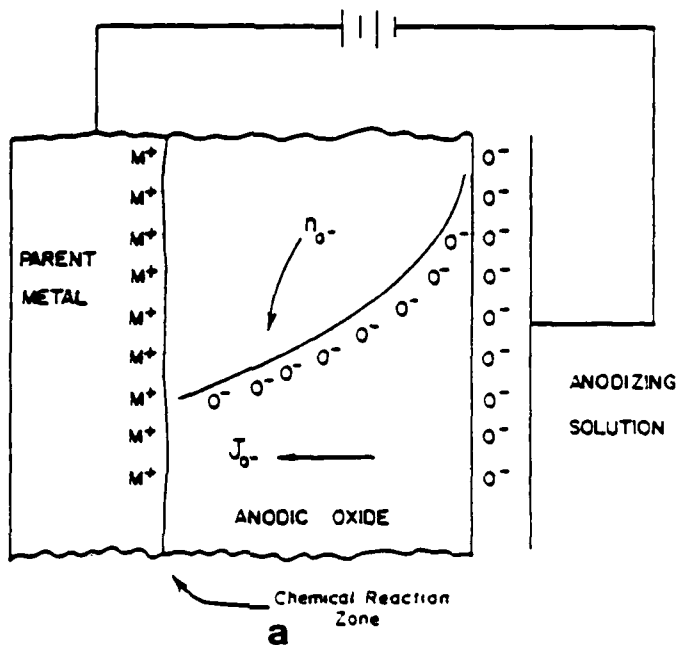


Figure 5: Oxide growth by (a) anion migration (b) cation migration. (Taken from [89])

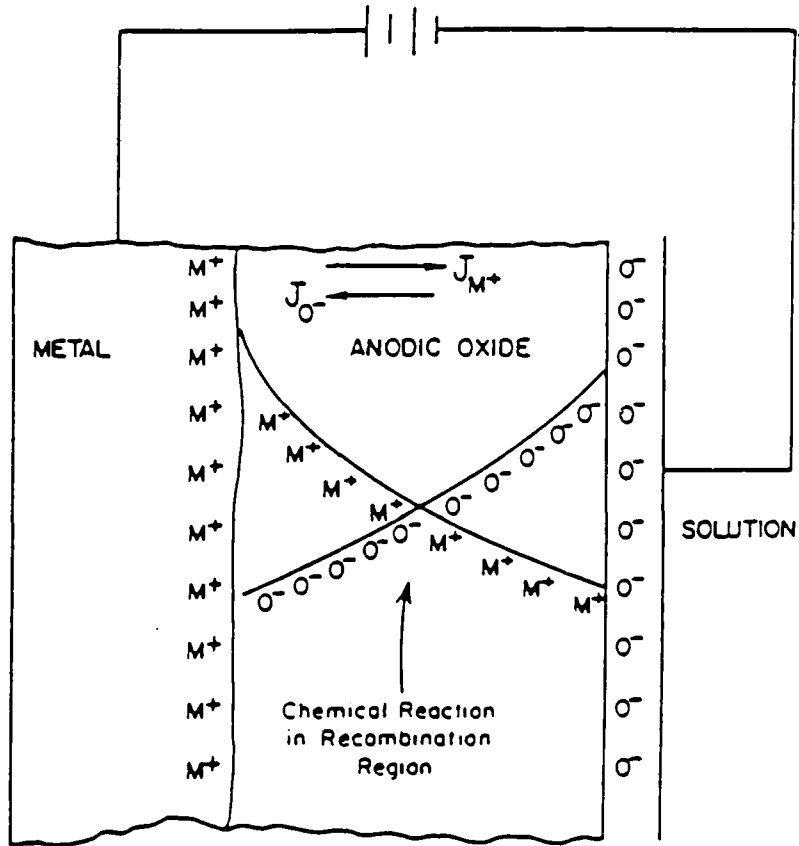


Figure 6: Oxide growth by joint cation and anion interstitial transport. (Taken from [89])

aluminum. Duplex films were formed by oxidizing in electrolytes of different concentration. It was reported that the last layer was formed on the oxide/solution side indicating that the metal ions are mobile. Vermilyea[50] also found that the metal ion to be the mobile species in Ta_2O_5 films anodized in 80wt% sulfuric acid.

There is evidence that both metal and oxygen ions can migrate simultaneously. Randall, Bernard and Wilkinson[51] formed duplex films on tantalum in various concentrations of phosphoric acid and found that fresh oxide layer were formed at both interfaces. Davies, Pringle and co-workers[52-54] obtained similar results for a number of valve metals including Al, Ta, Nb, Zr, Hf and W. Radioactive inert gases were used as markers in these studies.

The exact mechanism of ionic transport is difficult to elucidate. One must be cautious in using marker layers that the original transport mechanism is not altered and yet the marker layer must allow accurate identification. Therefore, the results are often dependent on the technique being used as well as the metal and electrolyte involved.

On the whole, there seems to be sufficient evidence that the metal ions are mobile in oxide formation. This is no surprise because they are smaller in size than their oxygen counterpart. In certain cases, both types of ions are

mobile, and oxide is formed by chemical recombination within the film and at the interfaces.

3.2 LIMITING OXIDE THICKNESS AND BREAKDOWN

As mentioned earlier, the final thickness of an anodic film is a function of the anodizing potential. However, due to a number of electrochemical as well as physical restrictions, the growth of the film is not unlimited. Oxide-breakdown or other electrochemical processes will take over, and further increase in potential or current density will not result in film thickening.

3.2.1 Internal Stress

It is generally believed that the oxide film formed anodically is under compression because the oxide occupies more volume than the metal from which it is formed. However, Vermilyea[55] found otherwise. He suggested that for a flat metal surface, the molecules should be able to rearrange while forming the oxide and therefore will not necessarily be in compression. He has shown by growing oxide on only one side of thin metal sheets that the oxide is actually under tensile stress. The exact state of stress within the oxide is difficult to quantify. It depends on a variety of factors such as metal surface, impurity, film

formation condition and film growth mechanism. Internal stress can be caused by flaws as pointed out by Vermilyea[56]. Internal stress due to space charge was reported by Fromhold[57]. Large stress can be induced by the migration of ions within the oxide during film growth. Electrostriction pressure is defined as the pressure exerted on the oxide due to the presence of high electric field which is in the order of 10^6 to 10^7 V/cm in anodization. This pressure alone, according to Sato[58], can exceed the breaking stress of most oxides as the oxide grows beyond a critical thickness and cause cracking. He pointed out also that the presence of strongly adsorbing anions which reduce the interfacial tension between the oxide and solution can lower the critical film cracking thickness. Hoar[59] reported that anion adsorption and penetration into the passive film may be a mechanism by which film cracking or splitting can occur. Piggott, Leckie and Shreir[60] reported that in anodizing Ti in formic acid, the presence of Cl^- lowers the pitting potential substantially in every case regardless of temperature or acid concentration.

3.2.2 Electrolytic and Dielectric Breakdown

Electrolytic breakdown can occur during the anodic process. Gradual breakdown was observed by Yahalom and Zahavi[61] for Ti anodized in H_2SO_4 . The cause of the breakdown is attributed to field-crystallization of the oxide. Dielectric breakdown occurs when voltage across the film becomes large. For an insulating oxide film, the separation between the valence band and the conduction band is sufficiently large. Electron current is not allowed at low potentials. However, at high enough potential, electron transition from valence band to the conduction band can occur by quantum mechanical tunneling. In such instances, appreciable electron current may flow across the film along with ionic current. Sparking may occur and lead to oxide burn-out.

3.2.3 Oxygen Evolution

The thickness of an anodic film can be limited even before cracking or sparking occurs. The thickening of the film depends on the potential gradient across the film. In potentiostatic anodization, the field will decrease drastically as the film thickens. Film growth will come to a practical halt in a short time. Further thickening of the film will require an increased potential. However, this

results in not only higher potential drop across the film, but also in the potential drop across the electric double-layer at the oxide/solution interface. As soon as the latter is great enough, new electrode processes can take place. In most cases, oxygen evolution will occur at the oxide/solution interface. The equilibrium potential for this process is +1.47 volt with respect to saturated calomel electrode (S.C.E.) [62]. Therefore, as soon as the potential difference at the double-layer exceeds say, -1.5, volt taking into account of overpotential, oxygen evolution will take place and further increase in potential will not increase field strength across the film, but only electrical current in the production of oxygen gas. Film growth will stop.

3.2.4 Oxide Dissolution

The thickness of the film is also limited by dissolution in the electrolyte. Dissolution is usually considered to be a chemical process rather than electrochemical. However, Vermilyea [63] reported that the dissolution rate of Ta_2O_5 in aqueous HF is directly proportional to the electric field. Nevertheless, dissolution rate is mainly a function of the oxide, electrolyte, pH, temperature, and mass transport around the oxide/solution interface. At the initial stage

of the oxide growth, the dissolution rate would be slower than the formation rate. As the oxide gets thicker, the field will decrease accordingly if the applied potential is held constant. Thus, at some thickness, the rate of formation will be in equilibrium with dissolution and thickening of oxide film will cease.

3.3 FORMATION OF POROUS OXIDE

It has been shown by Ditchek et al.[64] and Baun[65] that porous oxide can be obtained by anodizing Ti-6Al-4V in chromic acid. However, no mechanism as to how the pores were formed was offered. Venables et al.[66] showed high resolution SEM micrographs of the pore structure on aluminum anodized in phosphoric and chromic acids. An isometric drawing of oxide morphology for phosphoric acid anodized Al is shown in Figure 7. Wood[67] has provided a comprehensive review on the porous anodic oxide formation on aluminum.

Hoar and Yahalom[68] showed that when aluminum is anodized in acid solutions under constant potentials, the initial current density drop is associated with the formation of barrier layer oxide film. Subsequent gradual current rise to a maximum and to steady-state is associated with pore initiation and formation. These are evident from the electron micrographs taken at different stages of the

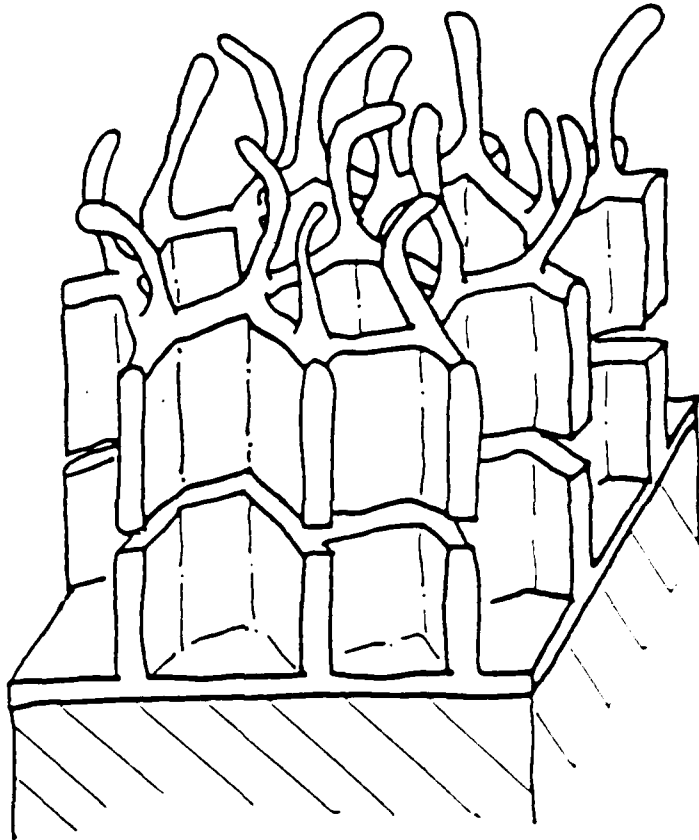


Figure 7: Isometric drawing of phosphoric acid anodized aluminum surface[66].

anodization. Pore formation is believed to be initiated by protons entering the film at random sites or grain boundary against the field. These sites create localized higher current density. This results in local Joule heating which, in turn, promotes more H^+ uptake and local dissolution. Once a pore is initiated, the high mobility Al^{3+} in the solution around the pore inhibit further H^+ uptake in the immediate region of the pore. This may explain the fact that the pores are well structured and equally spaced as observed from electron micrographs.

O'Sullivan and Wood[69] anodized aluminum in phosphoric acid under constant current densities. Pore formation was observed with transmission electron microscopy. Samples were taken from the different regions on the voltage-time curve. No pores were observed after 40 sec.. At 80 sec., the surface began to roughen. Further growth did not affect the surface topography, but beneath the surface, pores began to merge and increase in diameter. At 280 sec., steady-state pore size and distribution was reached. A model for pore initiation and formation was proposed. However, no satisfactory explanation was provided as to how the initial thinning of the oxide occurs which eventually leads to the observed transformation.

It was also pointed out that the cell-pore dimension is directly related by the forming voltage: larger pore size for higher forming voltage.

3.4 NATURE OF OXIDE ON TITANIUM

It is well accepted that the oxide present on anodized Ti surface is the tetravalent TiO_2 . Among the TiO_2 crystal modifications (rutile, anatase and brookite), rutile is believed to be the most stable form of TiO_2 due to its common occurrence. However, thermochemical data indicates that anatase is 8 KJ/mole more stable than rutile[27]. Furthermore, the hydrated form of rutile, $\text{TiO}_2 \cdot \text{H}_2\text{O}$, is also more thermodynamically stable than TiO_2 [70]

Yamaguchi[71] studied stripped oxide films on Ti anodized in H_2SO_4 by electron diffraction and found the oxide to be brookite. Electron diffraction was also used by Fraker and Ruff[72] to identify the film on Ti formed in saline water. Only anatase was found for films formed under 200°C .

Rutile, anatase as well as brookite were identified by Koizumi and Nakayama[73] on films formed on Ti in boiling dilute H_2SO_4 and HCl. Allen and Alsalim[74] reported that only rutile was present on Ti pre-treated by chemical etchings and sulphuric acid anodization. Yahalom and Zahavi[61] reported that the surface oxide on Ti anodized in H_2SO_4 to be anatase.

For chromic acid anodized Ti-6Al-4V, Natan and Venables[75] found the oxide to be mostly amorphous. There is no unanimity on the morphology of the anodic film on Ti or its alloy. There is little doubt that the oxide is titanium dioxide or some nonstoichiometric $TiO_{1.8-2.0}$ [88]. However, it appears that the film could be any one of the crystalline modifications or amorphous depending on the nature of the Ti metal or alloy, the electrolyte, forming voltage and current density.

3.5 OPTICAL PROPERTIES OF TITANIUM DIOXIDE FILMS

The anodic oxide on titanium shows brilliant interference colors depending on the oxidation conditions. It has been suggested that the color of the oxidized metal can be used to estimate the thickness of the oxide.

Baun[65] reported that as the voltage is stepped up at 10V increment in anodizing Ti-6Al-4V in H_3PO_4 , extremely vivid interference colors ranging from deep blue to brilliant gold were observed. Presumably, each time the voltage is increased, the oxide thickens correspondingly and give rise to the interference colors.

Briers[76] tabulated the color as a function of the TiO_2 film thickness on evaporated titanium (Table 2) The colors were calculated by using published optical constants for

TABLE 2

Interference color vs. oxide thickness for titanium[76]

Color	Oxide Thickness (nm)
weak grayish yellows	0-18
OLIVE BROWN	18-25
REDDISH BROWN	25-27
PURPLISH RED	27-30
PURPLE	30-35
BLUE	35-55
weak grayish greens	60-90
GREENISH YELLOW	95-105
GRAYISH ORANGE	110
PURPLISH RED	115-125
PURPLE	125-135
BLUE	135-145
BLUE-GREEN	145-160
GREEN	165-185
grayish yellows	185-195
pinks	195-210
PURPLISH RED	215-225

rutile. It should be pointed out that some colors repeat themselves as the thickness increases. Therefore, a particular color may indicate two different thicknesses. Also the determination of color is subject to interpretation by the observer, making visual estimation of thickness difficult.

Optical constants for polished bulk Ti and thermally grown oxide layers on bulk substrate was measured by Musa and Neal[77] by ellipsometry. Other authors[78-81] have also reported optical constants for titanium film and bulk titanium.

Chapter IV
EXPERIMENTAL

4.1 MATERIALS

Ti-6Al-4V is a alpha rich alpha-beta phase alloy at room temperature. The 6% aluminum increases the allotropic transformation temperature of titanium and strengthens the low temperature alpha (hexagonal close-packed) phase by solid solution. The 4% vanadium stabilizes the small amount of high temperature beta (body-centered cubic) phase at room temperature. All coupons used for anodization are commercial Ti-6Al-4V made by TIMET Corp. Typical chemical composition of the alloy is given in Table 3.

The coupons were measured 1" X 5" X .0025". Before anodization, all coupons were pickled in an acid solution made up of reagent grade HF and HNO₃ (Fisher Scientific). The chromic acid used as oxidizing electrolyte was made from reagent grade chromium trioxide crystals (Baker Chemical). Fifty grams of CrO₃ was dissolved into one liter of water. All solutions, including rinse-solution were made with double-distilled deionized water.

TABLE 3

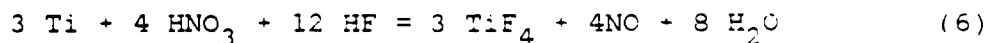
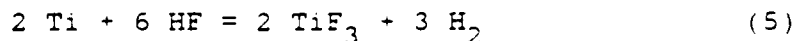
Chemical composition of the Ti-6Al-4V alloy

ELEMENT	MIN %	MAX %
Aluminum	5.50	6.75
Vanadium	3.50	4.50
Iron	----	0.30
Oxygen	----	0.20
Carbon	----	0.08
Nitrogen	----	0.015
Yttrium	----	0.005
Residual elements	----	0.40
Titanium	----	remainder

4.2 METHODS

4.2.1 Sample Preparation

The titanium coupons as received were grit-blasted to removed surface contamination and heat-treat scales. They were then wiped with methyl ethyl ketone or acetone to remove oil and grease contaminants. Acid pickling to remove pre-existing oxide was done by immersing the coupons in an 3% HF(49%), 15% HNO₃(70%) solution. Pickling time was one minute unless otherwise stated. The exact concentration of the nitric and hydrofluoric acid is not as important as the 10:1 ratio[82]. The oxide on titanium will dissolve readily in HF. However, the free hydrogen generated in the reaction as shown in Equation (5) can cause hydrogen embrittlement in the metal. The presence of excess HNO₃ with HF tends to inhibit the generation and absorption of hydrogen through the oxidation reaction shown in Equation (6).



After pickling, the coupon was immediately rinsed in distilled water and wiped dry with Kimwipes[®]. The coupons

were then transferred to the anodizing bath as soon as possible (usually less than 1 min.) to minimize oxidation before anodization.

4.2.2 Apparatus

The schematic of the apparatus for anodization is shown in Figure 8 and Figure 9. A potentiostat/galvanostat (Model 173 EG&G Princeton Applied Research) was used along with a current follower (Model 176 EG&G Princeton Applied Research) and an electrometer (Model 178 EG&G Princeton Applied Research) to provide either constant potential or constant current for the anodization. The current and potential output was recorded by a Fisher Recordall series 5000 two-pen strip-chart recorder.

Chromic acid (0.5 M) was placed in a 2-liter polypropylene container. The electrolyte was agitated by a magnetic stirrer while the temperature was monitored by a mercury thermometer. The experiments were carried out at ambient temperature ($\approx 28^{\circ}\text{C}$). The reference electrode was a saturated KCl saturated calomel electrode (Fisher Scientific). An auxiliary D.C. power supply (Heath/Schlumberger Model SP-2731) was used in series with the potentiostat to increase the upper potential limit of the potentiostat from 4.999 V to 11.5 V operating in the

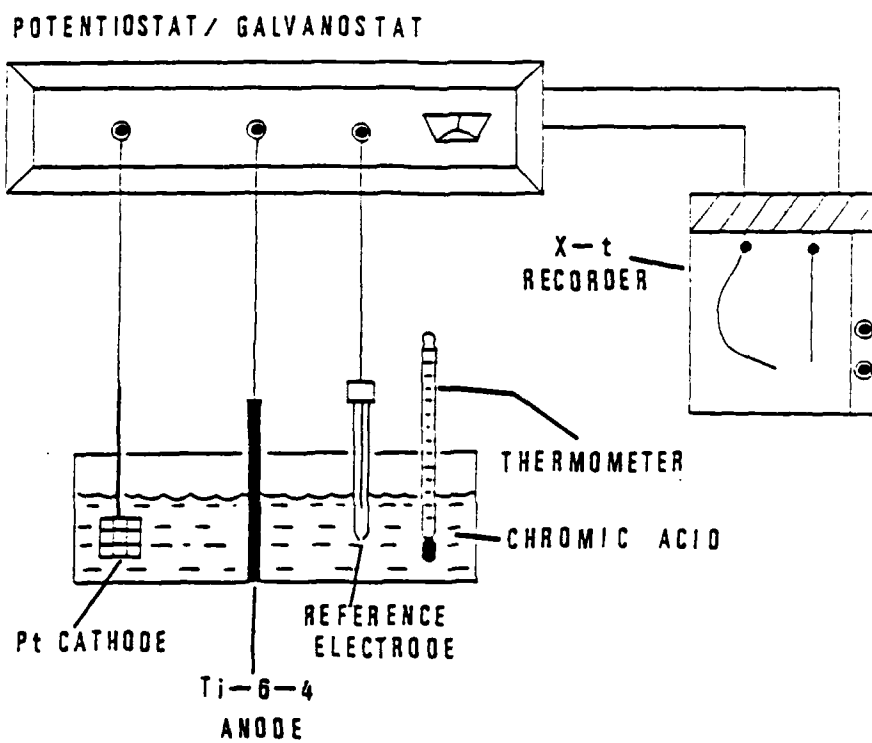
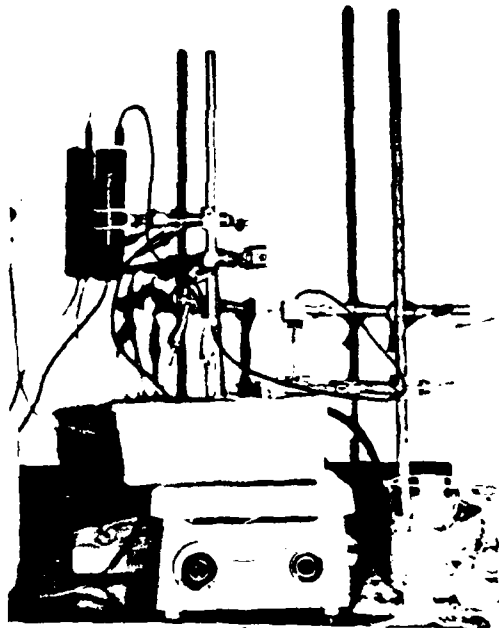


Figure 8: Schematic of anodization apparatus



a



b

Figure 9: Anodization apparatus. (a) potentiostat and recorder (b) anodization bath.

potentiostatic mode. A platinum gauze was used as counter electrode while Ti-6-4 was connected to the anode.

The potentiostat has a current capability of one ampere and built-in voltage source of ± 4.999 V. External potential sources can be added to enhance the potential range. In the potentiostatic mode, the potential is adjustable from 0 V to 4.999 V with ± 1 mV resolution and tolerance of $0.1\% \pm 1$ mV. In the galvanostatic mode, current from 1 μ A to 1 A can be selected with tolerance of $0.1\% \pm 100$ ppm/ $^{\circ}$ C from 1 μ A to 10 mA, and $0.2\% \pm 100$ ppm/ $^{\circ}$ C from 100 mA to 1 A.

High resolution electron micrographs were made possible by using a PHILIPS EM-420 scanning transmission electron microscope (STEM) operating in the scanning mode. For the Ti-6-4 samples, micrographs with magnification up to 200,000X with good resolution were obtained without the need for a conductive coating. Photomicrographs were also obtained using a JEOL JSM-35C scanning electron microscope (SEM) for some samples. However, in these cases, magnification was limited to about 18,000X, and a Au-Pd coating was required. Some micrographs were taken in stereo pairs with a 4° tilt. When looking at the stereo pairs through a stereo viewer, one can easily resolve the fine topographical features from the threedimensional images.

4.2.3 Galvanostatic Anodization

The pre-anodization sample preparation is described in Section 4.2.1. Anodic charging curves were obtained by anodizing the coupons at different current densities. The coupons used in this part of the experiment were not grit-blasted each time before they were pickled and anodized. An as-received coupon was pickled for at least five minutes at the beginning to obtain a smooth and uniform surface. The same coupon was then used to obtain a set of charging curves with one-minute pickling in-between anodization. This was done because the "true" surface area may be quite different for grit-blasted samples with the same "apparent" surface area. This may lead to erroneous current density calculations.

In the galvanostatic mode the current density is simply the total current divided by the "apparent" surface area. The potentiostat/galvanostat maintains a constant current flow by continuously varying the potential of the cathode. The potential transient was output to the recorder and potential-time curves were obtained.

The advantage of using galvanostatic method in studying anodic oxide growth is that the total charge passing through the oxide is directly proportional to the time of anodization. If the current efficiency, which is the

percentage of current directly contributed to forming the oxide, is close to 100%, one can easily calculate the volume and the thickness of the oxide film at any time using Faraday's law. Furthermore, the field strength (H) within the oxide will remain constant as the oxide thickens. This allows convenient calculation of kinetics parameters as shown in the Appendix.

4.2.4 Potentiostatic Anodization

In this mode of operation, the potentiostat maintains a constant potential difference between the reference electrode and the titanium anode. The current flow between the cathode and anode was measured and plotted as a function of time on the recorder.

Chromic acid anodization (CAA) of Ti-6-4 is conducted under constant potential condition in industry[87]. In fact, the anodization is usually carried out at a constant 10 V by a D.C. power supply at ambient temperature. Current density is adjusted to 1.5 to 2.5 A/ft² by the addition of small amount of HF. It was shown that highly porous TiO₂ oxide film can be obtained under these conditions[64,65]. Therefore, present effort will be focused on the formation of this oxide under different voltage, temperature and time of anodization as well as the role of HF in the process.

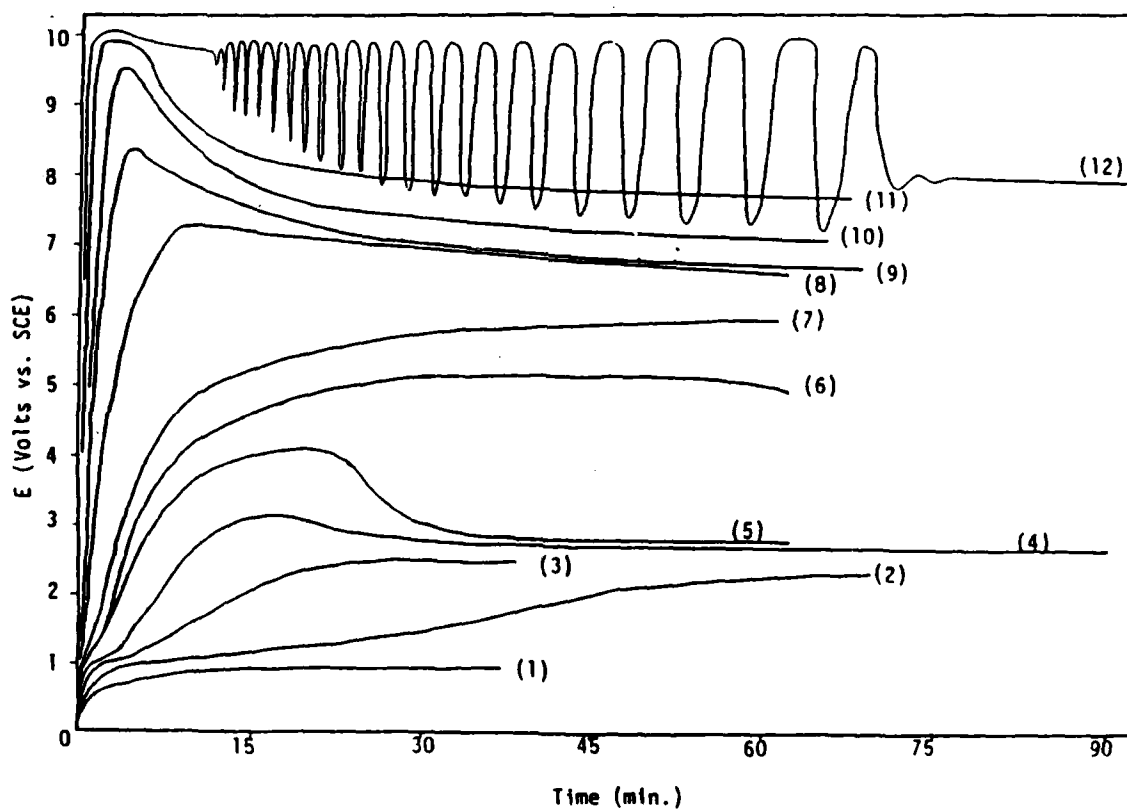
The presence of fluoride on the oxide of aluminum has been shown to have deleterious effect on joint strength[89]. It is not clear if the same is true for titanium.

Chapter V

RESULTS AND DISCUSSION

5.1 GALVANOSTATIC ANODIZATION

The potential-time curves for current density (CD) from 3.28 $\mu\text{A}/\text{cm}^2$ to 1.82 mA/cm^2 for Ti-6-4 anodized in 0.5M chromic acid solution are shown in Figure 10. In almost all cases, the curves initially rose linearly with slopes dependent on CD, and either reach a maximum and come to a steady-state voltage or continuously rise approaching a steady-state potential. This is consistent with charging curves reported elsewhere for Ti[46, 39, 60] and Al[84, 85]. Markedly different from other curves is curve (12) in Figure 10. After reaching 10 V and began to steady out, the potential started to oscillate in a cyclic fashion. For CD slightly above 1.82 mA/cm^2 , similar curves were obtained. It is likely that the oxide underwent cracking under the high field. When the oxide cracks, the potential dropped because of the low resistance path for current flow. However, the cracks would be repaired quickly, and the potential would rise until cracking occurred again. This explains the rise and fall in the potential-time curve. For CD much higher than that, pitting and oxide cracking occurred (Figure 11) with rapid oxygen evolution. In this instance, the ionized



Plot of potential vs. time curves at different current densities in 0.5M chromic acid solution.

(1) 3.28 $\mu\text{A}/\text{cm}^2$	(2) 14.6 $\mu\text{A}/\text{cm}^2$	(3) 32.8 $\mu\text{A}/\text{cm}^2$	(4) 54.7 $\mu\text{A}/\text{cm}^2$
(5) 91.1 $\mu\text{A}/\text{cm}^2$	(6) 0.11 mA/cm^2	(7) 0.15 mA/cm^2	(8) 0.33 mA/cm^2
(9) 0.51 mA/cm^2	(10) 0.73 mA/cm^2	(11) 1.46 mA/cm^2	(12) 1.62 mA/cm^2

Figure 10: Potential vs. time curves at constant CD.



Figure 11: SEM Photomicrographs showing cracked oxide at a pit formed under high CD or above 10 V.

metal at the pits or cracks was accelerated so fast under the field that oxide could literally be forming in the electrolyte some distance from the oxide layer. The pits will therefore continually deepen without a chance to heal. Oxide cracking can occur due to a number of reasons, viz, electrostriction pressure, internal compressive/tensile stresses, ionic migration and flaws.

As the potential approaches 10 V, rapid gas evolution is visible on the oxide surface. It is evident that oxygen evolution becomes dominant at 10 V. Even at 9 V or below, very fine bubbles are present on the oxide surface.

The oscillation in curve (12) is not the consequence of instrument instability or reference electrode contamination. Oxygen rapidly evolves from the anode surface when the potential reaches 10 V but ceases as the curve drops to the trough of the cycles at 8 to 9 V. This indicates that the field across the oxide film does indeed vary during each cycle of the oscillation.

Figure 12 and Figure 13 depict the $E/\log I$ relation at 20 min. and 60 min. of anodization time, respectively. A distinct transition was observed in both cases at CD around 10^{-4} A/cm². The implication is that either the conductivity for current flow suddenly decreases, or the resistance increases when the CD goes from 10^{-5} A/cm² to 10^{-3} A/cm².

This transition might be the result of a change in the nature of the film leading to lower conductivity.

A comparison of an ideal charging curve and a typical charging curve is illustrated in Figure 14. The ideal curve begins with a linear potential rise which is attributed to oxide growth at 100% current efficiency. The slope of the linear region is dependent on CD. At V_1 , a competing electrode process, such as oxygen evolution, begins to take effect causing the slope to decrease due to lower current efficiency. At V_2 , oxygen evolution or oxide breakdown completely dominates the electrode process and the voltage reaches steady-state. The dashed curve represents a typical experimental charging curve. The initial potential rise is probably due to charging of the electric double-layer or adsorption of oxygen on the surface. Subsequent linear rise is due to oxide growth and eventually reaching the steady-state without a pronounced transition.

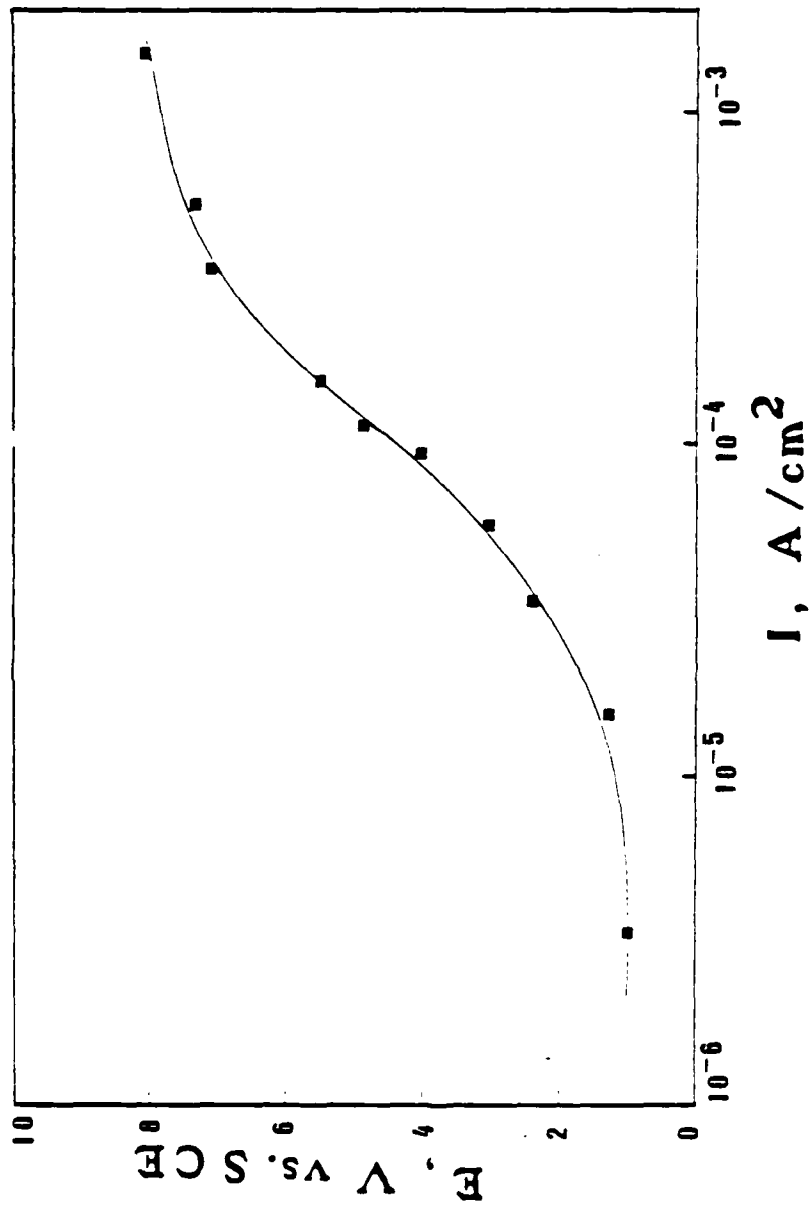


Figure 12: POTENTIAL, E VS. $\log I$ at anodizing time of 20 min..

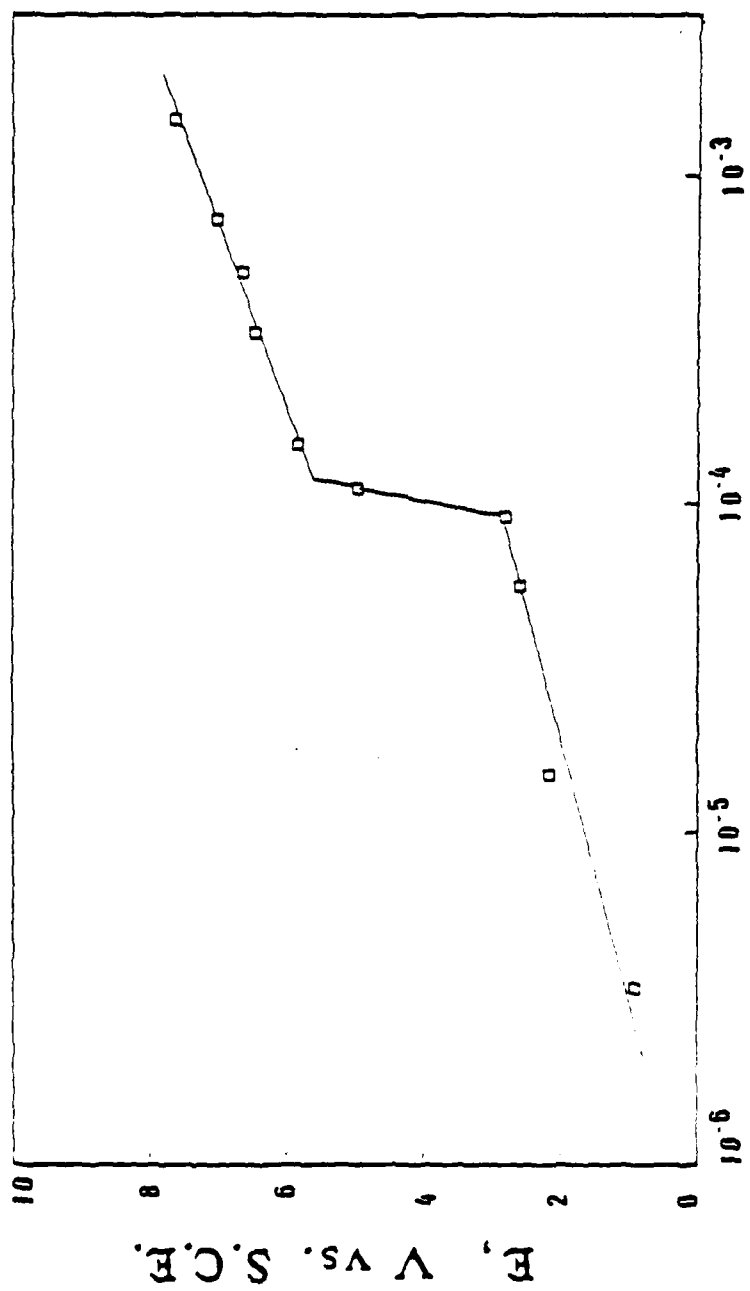


Figure 13: POTENTIAL, E vs. LOG I at anodizing time of 60 min..

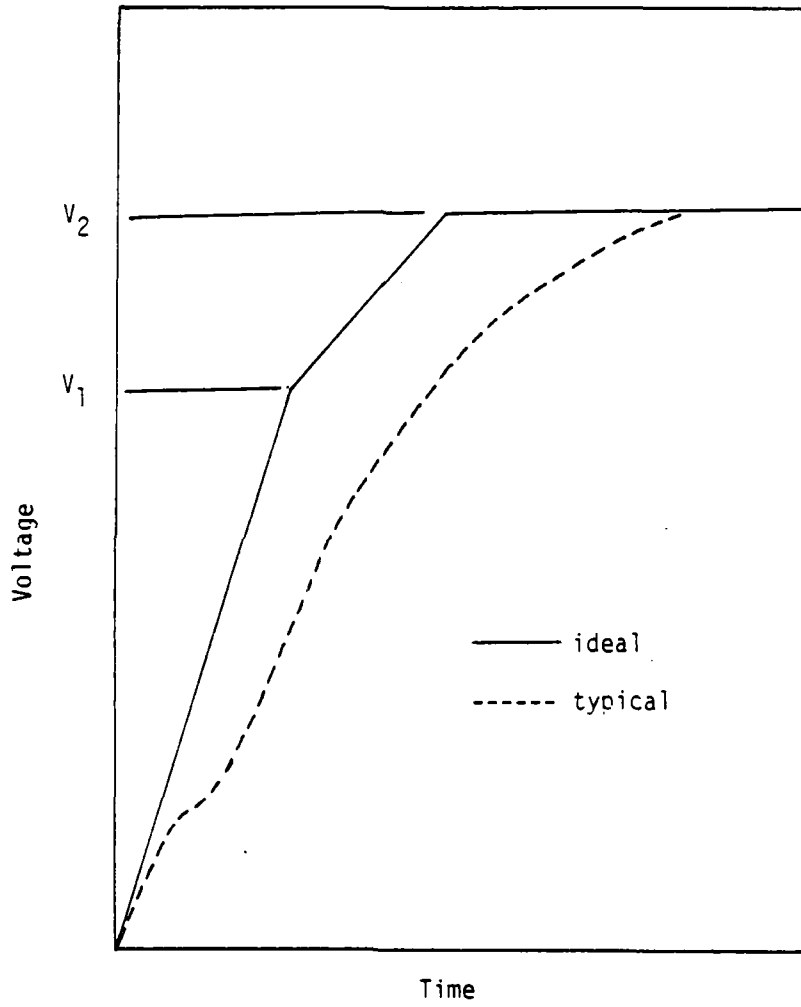


Figure 14: Comparison of an ideal and a typical voltage/time curve.

5.2 CALCULATION OF ELECTROKINETIC PARAMETERS

All calculations were based on the linear oxide growth region of the charging curves only. Additional experiments were performed in the oxide growth period to obtain more accurate slopes than the ones shown on Figure 10. At the linear region of the charging curves, the current efficiency is close to 100% and the amount of oxide deposited can be calculated from the charge passed. Detailed derivation for the calculations is included in Appendix A. In the following discussion, the equations are referring to the ones in the Appendix.

For most valve metals, the steady oxide formation rate is related to the apparent anodic current density by the empirical relation:

$$(dE/dt)_I = a I^b$$

where a and b are constants. This relation was found by Johansen et al.[40] to apply to the anodization of Al, Ti, Hf, V, Nb and Ta. Ammar and Kamal[46] also found this to apply for acid anodization of Ti. Figure 15 shows the relation between $\log(dE/dt)_I$ and $\log I$ for the present study

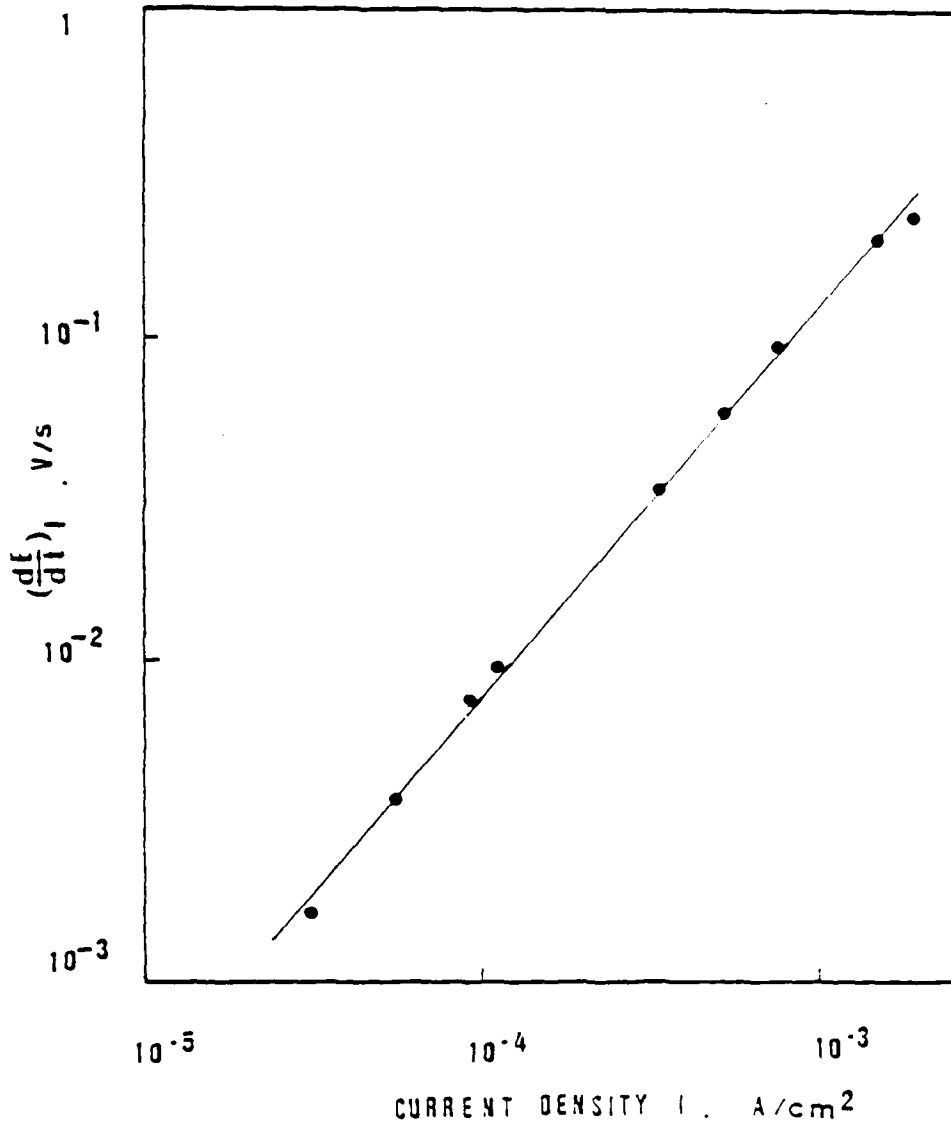


Figure 15: $\log(dE/dt)_I$ vs. $\log I$

on Ti-6-4. The constants a and b calculated from the slope and intercept of Figure 15 are $758.6 \text{ (cm}^2/\text{farad)(cm}^2/\text{A)}^{0.25}$ and 1.25, respectively. The constant a was found to decrease with pH while b was independent of the electrolyte or pH[85].

Equation (17) shows that the plot of $(1/I)(dE/dt)_t$ vs. $\log I$ will give a straight line as depicted by Figure 16. With $n=4$, $\rho = 4.1 \text{ gm/cm}^3$ [86] and $M = 79.9 \text{ gm/mole}$ for TiO_2 , the electrolytic parameter A was calculated from the intercept to be $2.31 \times 10^{-6} \text{ A/cm}^2$. Without having to estimate the roughness factor, σ , σ_B was calculated from the slope to be $2.3 \times 10^6 \text{ cm/V}$. The order of magnitude of these parameters is consistent with those reported earlier[46, 85, 40]. The parameter A was reported to be inversely proportional to the height of the potential energy barrier for ion migration and increase with pH[40,46]

Equation (21) from Appendix A indicates that the plot of $(dE/d \ln I)_t$ vs. $\log I$ is non-linear with slope increasing with increasing I . This behavior is shown in Figure 17. However, if the $E/\log I$ relation was plotted at constant charge density, Q , according to equation (23), a straight line can be obtained, and from the slope and intercept, the pre-immersion oxide thickness, δ_0 , can be calculated. It is reasonable to assume that δ_0 does not vary much between

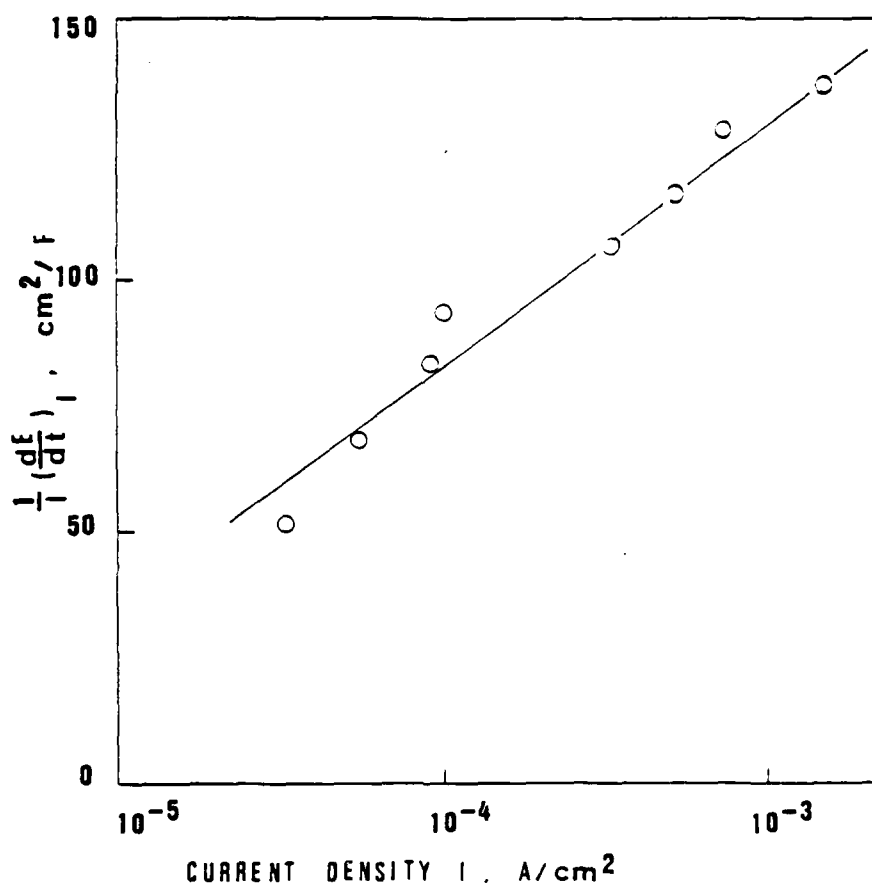


Figure 16: Unitary formation rate, $(1/I) \{dE/dt\}_I$, vs. $\log I$

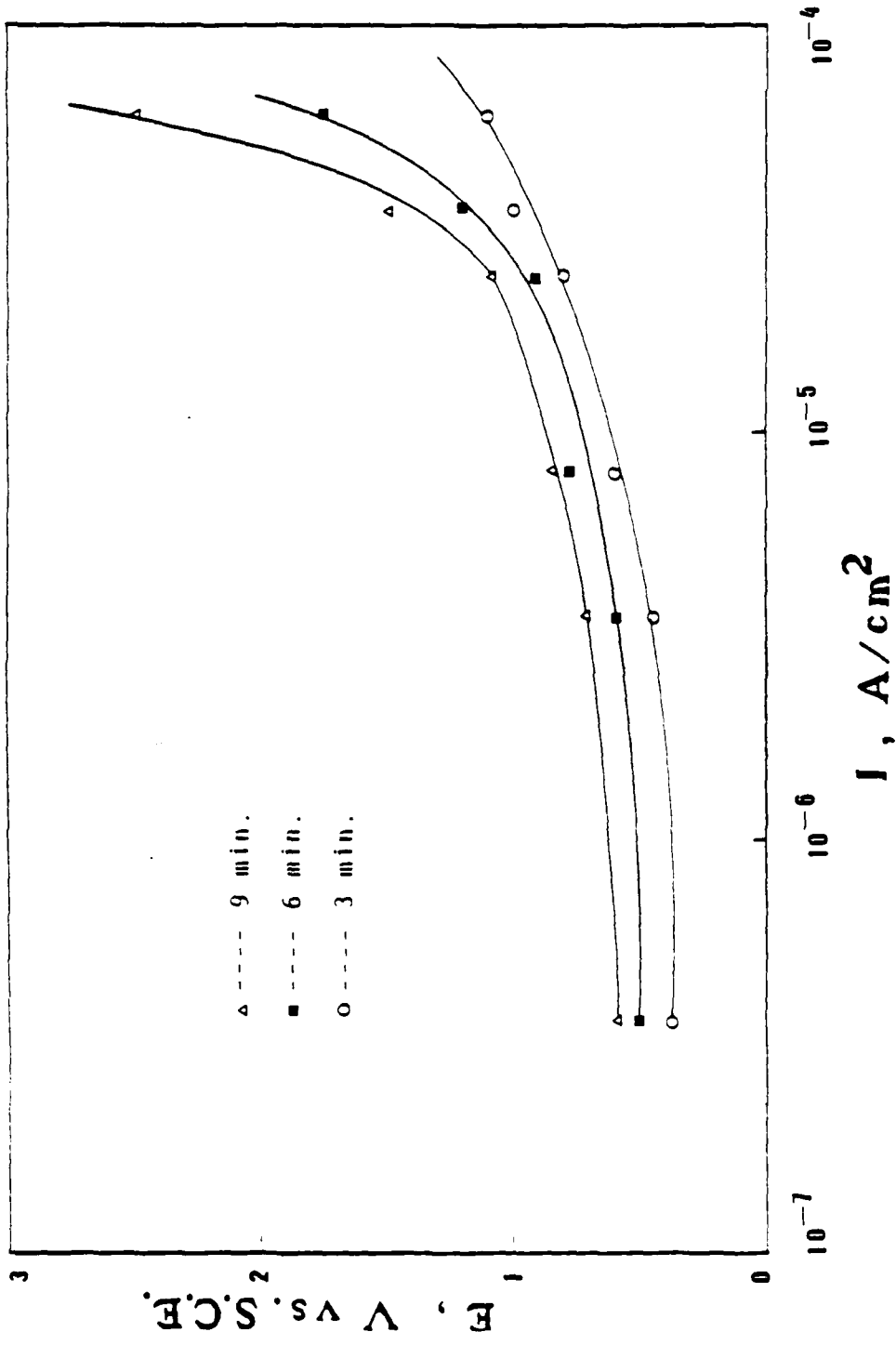
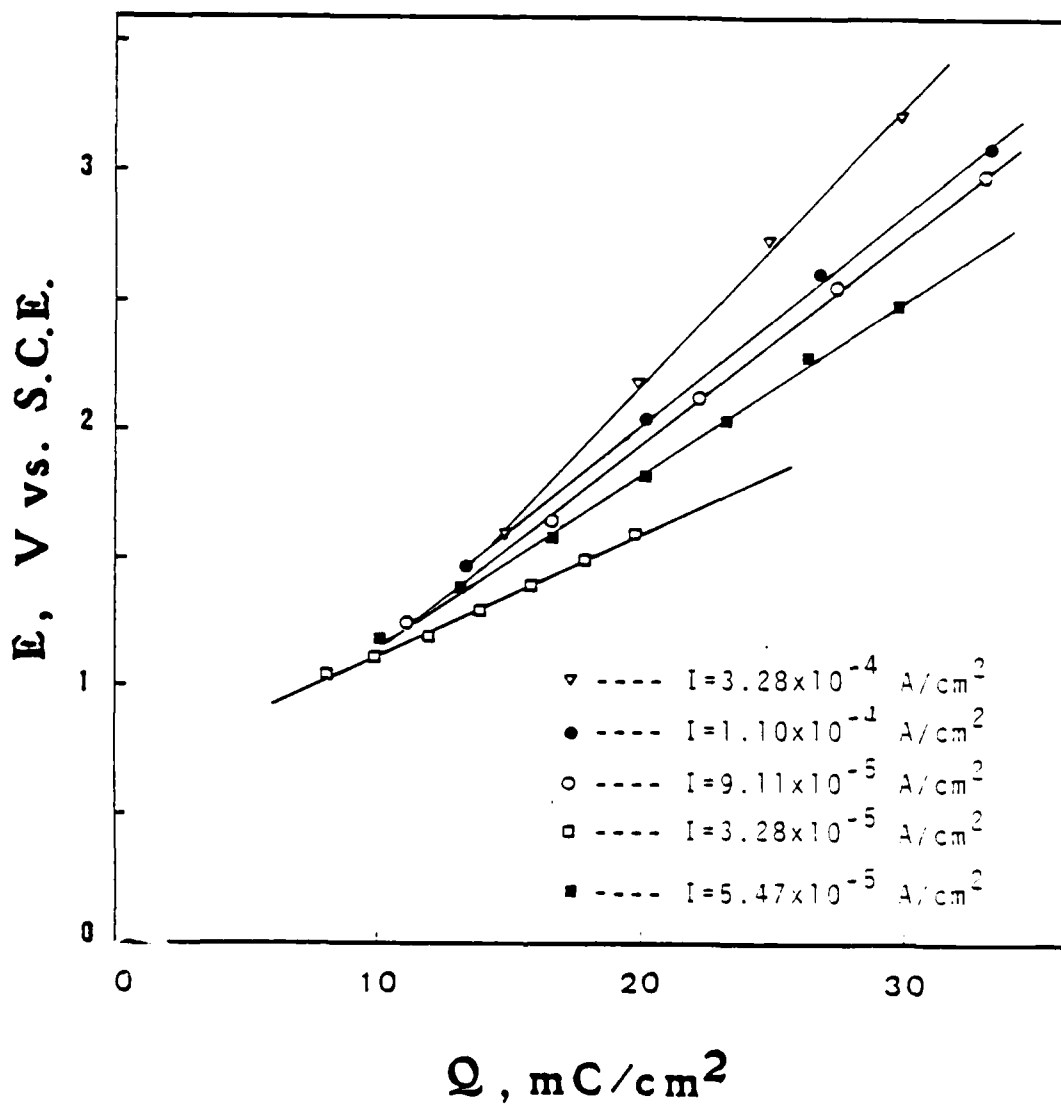


Figure 17: Plot of POTENTIAL, E vs. I at constant anodizing times of 3 min., 6 min., and 9 min.

experiments when the same sample preparation technique is followed.

In order to get $E/\log I$ relation at constant Q , Figure 18 was first constructed. From Figure 18, $E/\log I$ data were obtained at constant Q and are plotted as in Figure 19. Assuming the roughness factor, $\sigma = 5$, the pre-immersion oxide thickness, δ_o , is calculated to be in the order of 10 Angstrom/V. This number is slightly higher than the 4-5 Angstrom/V reported by Ammar and Kamal[46] on Ti. The difference can easily be accounted for by the difference in the nature of the metal and sample preparation technique.

Figure 18: E/Q relation at constant I .

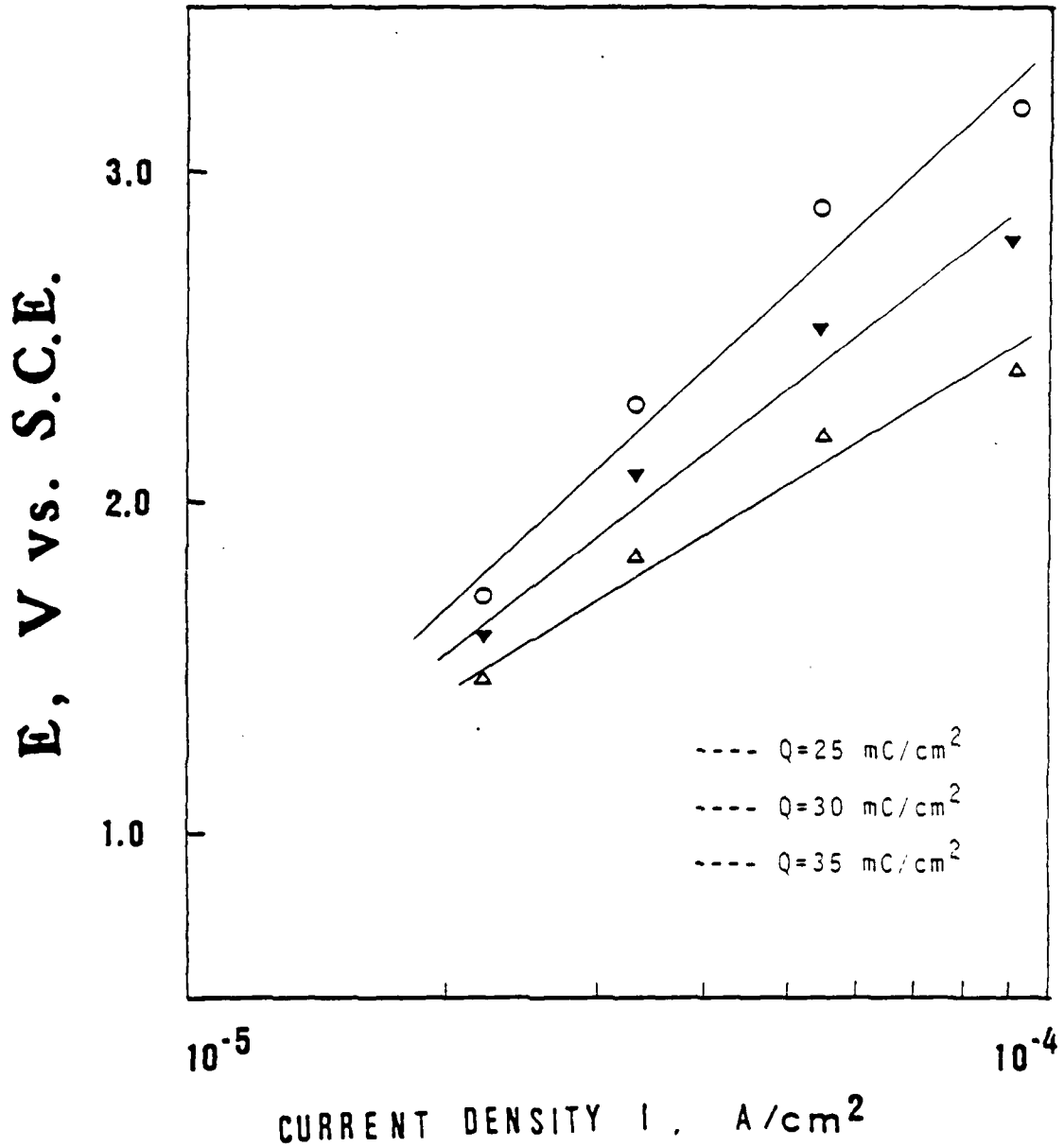


Figure 19: E/log I relation at constant Q.

5.3 POTENTIOSTATIC ANODIZATION

Since commercial anodization is done by applying a constant 10 V across the anode and cathode, both of which made of Ti-6-4, it is instructive to compare the difference between the applied voltage from a D.C. power supply and voltage as measured by a potentiostat referencing to a calomel electrode. Figure 20 illustrates the results obtained by applying a constant voltage via a power supply across the Ti-6-4 anode and cathode and measuring the potential in the solution against the calomel electrode. The two voltages were almost in perfect agreement. Therefore, it is safe to say that the current/potential readings from the potentiostat used in this study are directly translatable to those obtained in the more simplistic commercial set-up.

Figure 21 shows the current transient curves under constant voltage. In all cases, the curve immediately dropped to a minimum within the first minute or less. It was followed by a gradual increase in current. These results are consistent with the ones obtained by Hoar and Yahalom[68]. In the initial minutes, the formation of a barrier layer is responsible for the current drop. Beyond this point, the current gradually rises at a rate depending on the applied voltage. Hoar and Yahalom attributed this

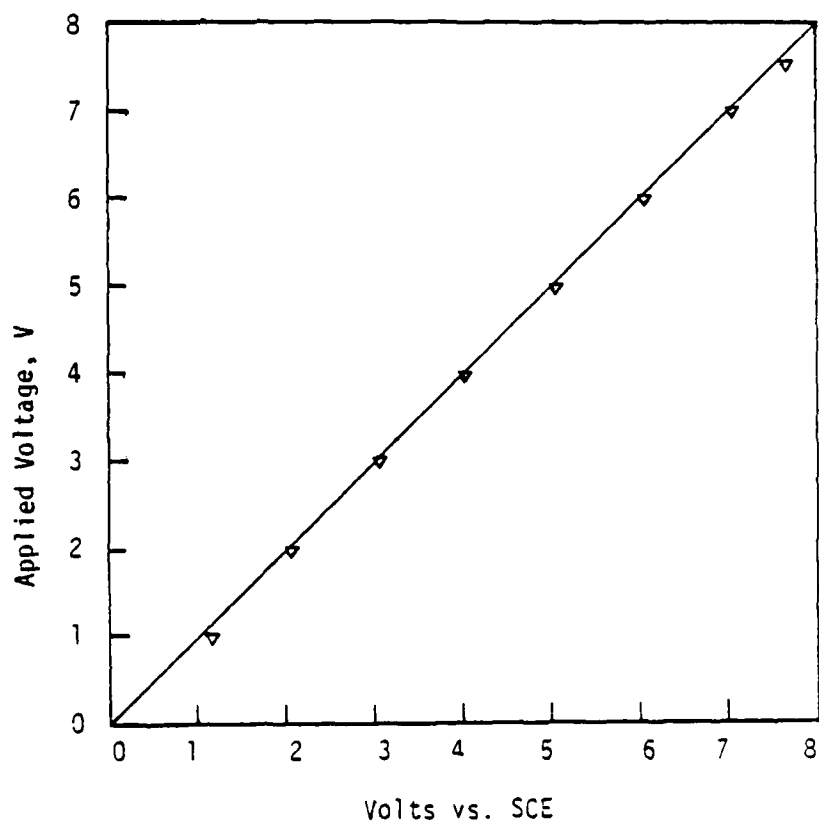


Figure 20: Applied voltage vs. voltage measured against SCE.

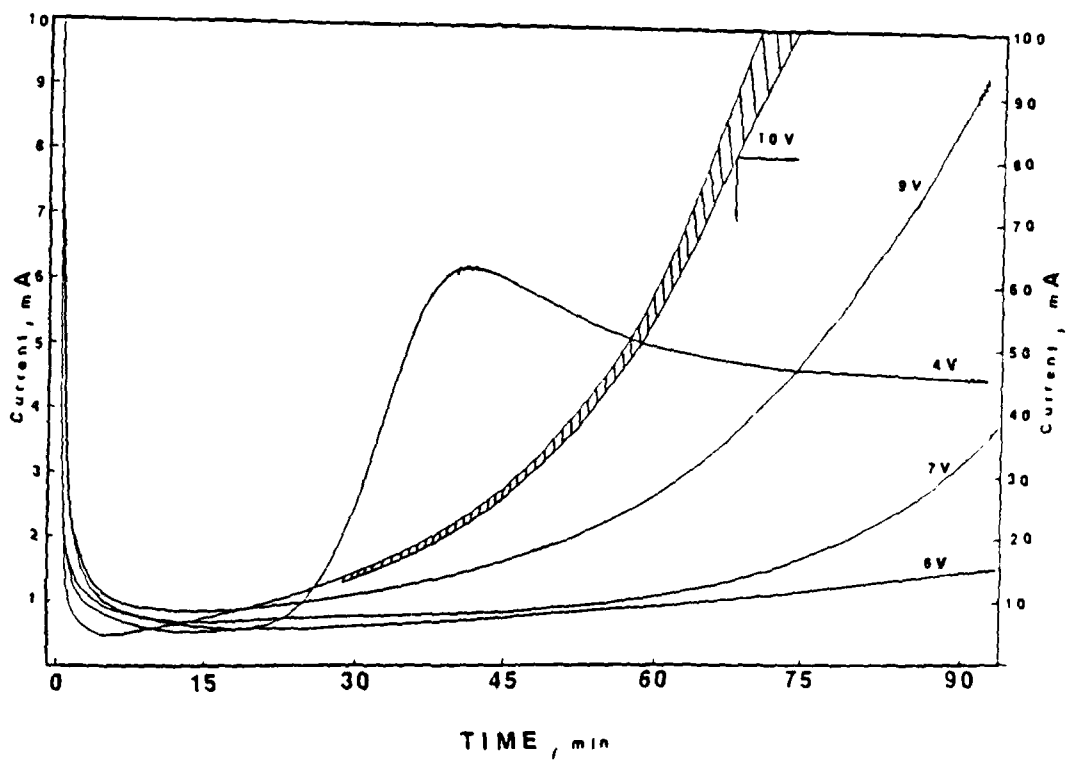


Figure 21: Current/time relation under constant potential.

phenomenon to the initiation and formation of pores. They reasoned that after the barrier layer is formed, film growth will almost come to a stand-still. Thermally enhanced protons from the electrolyte can enter the film against the field and cause localized current increase. Higher current leads to Joule heating and thus faster dissolution at localized spots. Faster dissolution will in turn increase current flow and, thus, the process is self-sustaining. Since the pore base is thinner than the barrier layer initially formed, this could very well explain the upturn in the current transient. However, there are other mechanisms by which one can explain this phenomenon.

As mentioned in Chapter 3, electrical current will compete with ionic current as soon as the potential difference at the oxide interface reaches 1.5 V where oxygen evolution is possible. It is likely that the current rise merely reflects the increase in electrical current in forming oxygen gas. Oxide cracking, which is evident from the current fluctuation at 10 V, will increase electrical current flow as well. It should be emphasized that the current rise at 10 V is much faster than that at 9 V and below.

5.4 EFFECT OF HF, TIME AND TEMPERATURE ON OXIDE MORPHOLOGY

Hydrofluoric acid is used to increase current density during chromic acid anodization in commercial process. However, the exact role of the HF in the final oxide topography is unclear. Samples used in this section were all anodized at 10 V and for 20 minutes at ambient temperature unless otherwise stated.

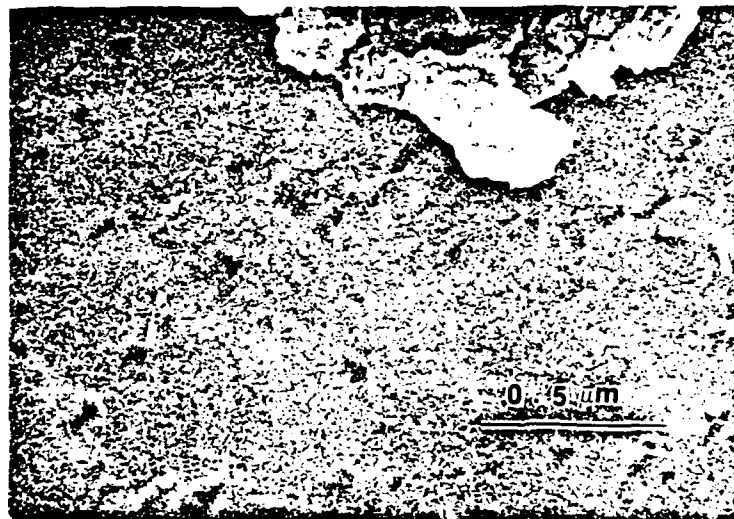
Scanning (transmission) electron microscopy (STEM and SEM) were used to study the surface topography of the oxide layer on Ti-6-4 formed under various conditions.

Figure 22a shows a STEM micrograph of Ti-6-4 anodized in chromic acid under constant current condition. In Figure 22b, the sample was anodized under constant current until the voltage reached its peak at 10 V, it was then switched to constant 10 V. In both cases, the anodizing time was 20 minutes and without HF addition. There is no topographical difference between the two samples, and the oxide films appear to be pore-free and uniform throughout.

STEM micrographs comparing surfaces anodized for 2 and 20 minutes at 10 V with HF are shown in Figure 23 and Figure 24, respectively. Figure 25 shows the same surface as in Figure 24 except in higher magnifications to review the pore structure. The surface topography was even more vivid when viewing the micrographs in stereo pairs under a stereoc



a



b

Figure 22: STEM photomicrographs of anodized Ti-6-4 surfaces. (a) at constant current density $i=1.35 \text{ mA cm}^{-2}$ (1.25 A/ft^2). (b) at constant $i=1.35 \text{ mA cm}^{-2}$ until the voltage reached 10 V then switched to constant potential. total anodizing time in both cases is 20 minutes. $150,000\times$

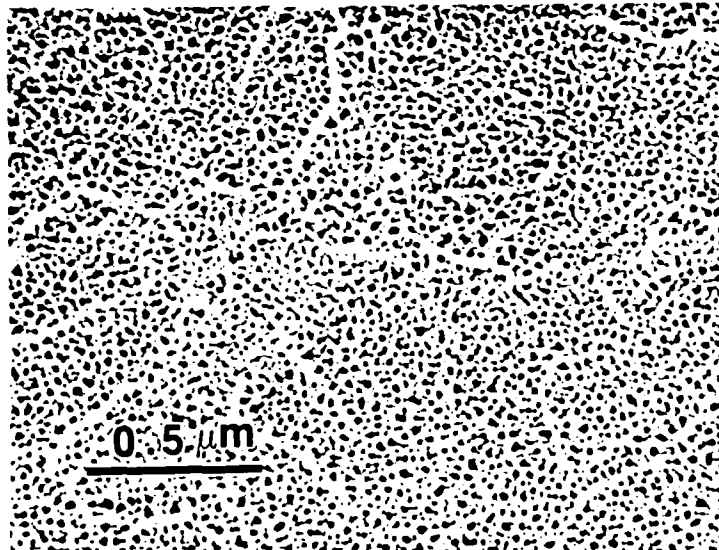
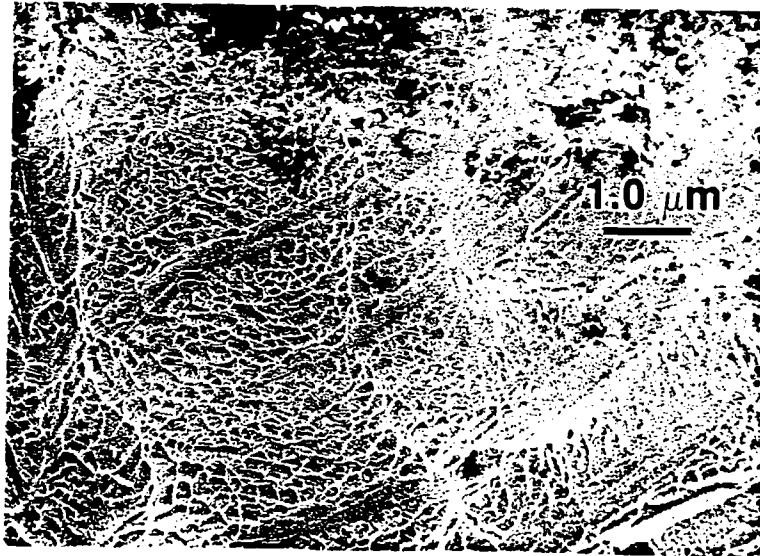


Figure 23: STEM photomicrographs of CAA Ti-6-4 at 10 V for 2 minutes with HF addition.

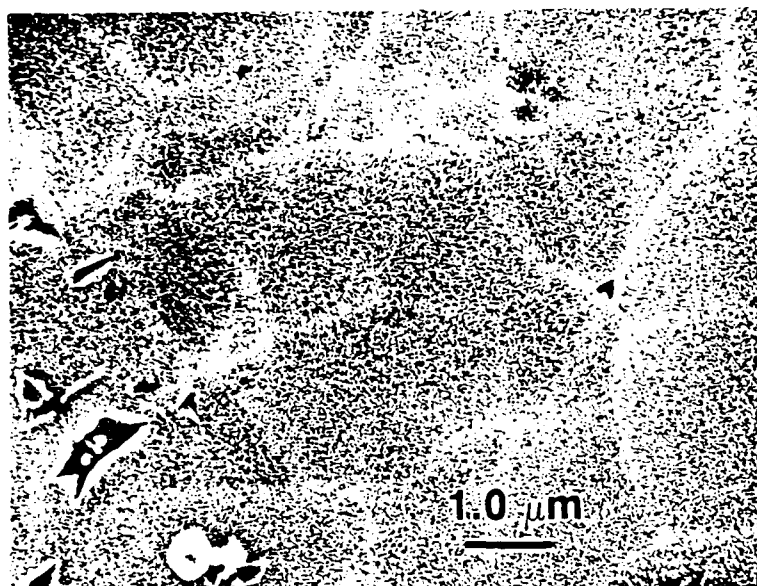


Figure 24: STEM photomicrographs of CAA Ti-6-4 at 10 V for 20 minutes with HF addition.

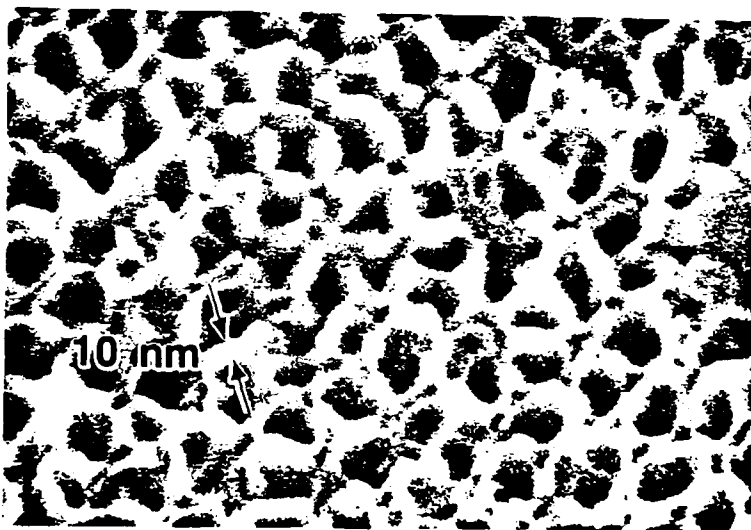
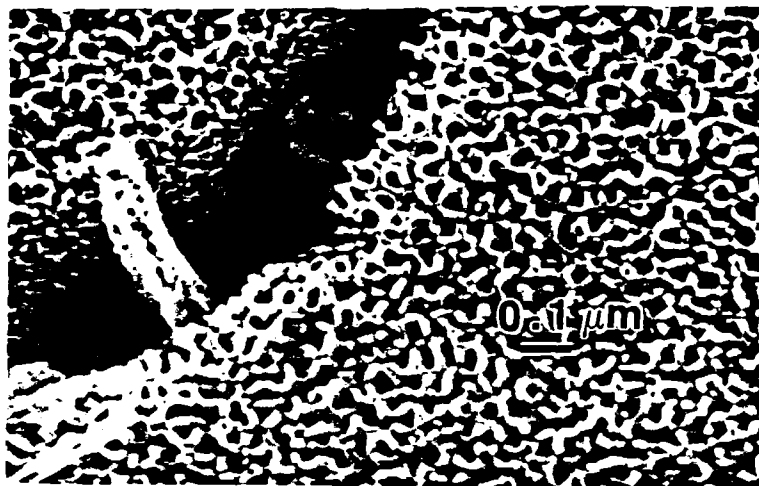


Figure 25: STEM photomicrographs of CAA Ti-6-4 at 10 V for 20 minutes with HF addition. (high magnifications)

viewer. These pores resemble those reported by Venables et al. [66] (Figure 9) for phosphoric acid anodized Al surface. The pore size is rather uniform with cell diameter of 10-20 nm. The finger-like protrusions on the surface as shown in Figure 25a are in the order of 25-50 nm. The crevice or depressed regions are probably a result of preferential etching of the beta phase alloy during either the acid pickling or the anodizing step.

The surface anodized for 2 minutes showed pore structure as well as surface roughness while at 20 minutes, it was relatively smooth aside from the pores themselves.

For illustration purpose, the surface of a phosphate-fluoride etched sample was include in Figure 26. No porosity was observed on this chemically etched surface.

Figure 27 and 28 depict an oxide formed at 54°C under current density about twice as much as other samples through adding extra amount of HF. Again, pores similar to those in Figure 24 and Figure 25 were present. However, the diameter of the pores were seven to ten times larger.

Figure 29, Figure 30, and Figure 31 show the comparison between oxide surfaces anodized at 8, 9, and 10 V respectively, with and without HF addition. In all three cases, it is evident that pores are present only on surfaces anodized with the addition of HF to adjust the current

density. Because of the limited resolution of the SEM micrographs at such magnifications, it is not possible to compare the pore structure other than to identify their presence. In Figure 32, for the sample anodized for 16 minutes instead of 20 minutes, there was surface roughness plus porosity in the case with HF, but again only a smooth compact film was obtained when no HF was added. The roughness pattern was somewhat similar to that of the sample shown in Figure 23.

It can be summarized from the STEM and SEM micrographs that when anodizing for 20 minutes or less, the oxide was uniform and compact in all cases. In cases where HF was added, regardless of anodizing time, temperature and voltage, porous oxide resulted. Samples anodized for less than 20 minutes in the presence of HF showed irregular surface roughness along with porous structure. Samples anodized according to the commercial process at 10 V for 20 minutes with the addition of HF to adjust the current density to 1.5-2.5 A/ft² yielded a highly regular pore structure with fairly uniform pore size distribution, not unlike the structure for aluminum anodized in phosphoric acid.

There is a particular interference color associated with certain oxide thickness. In the absence of HF, the

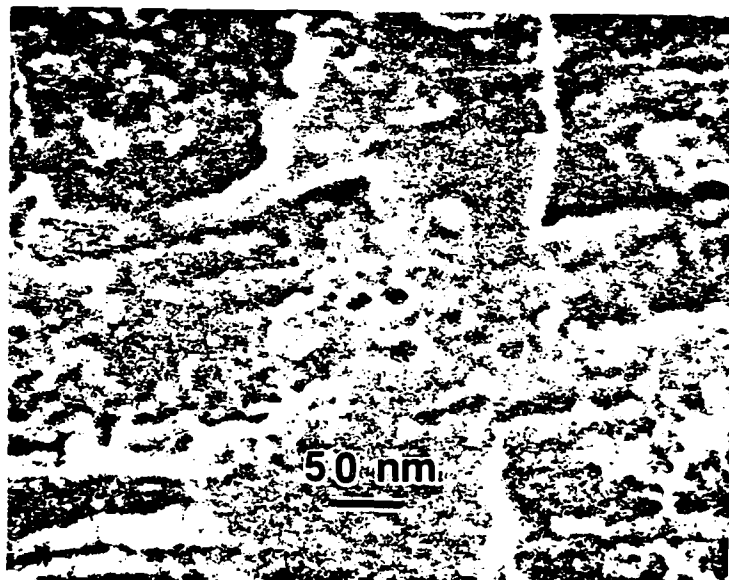
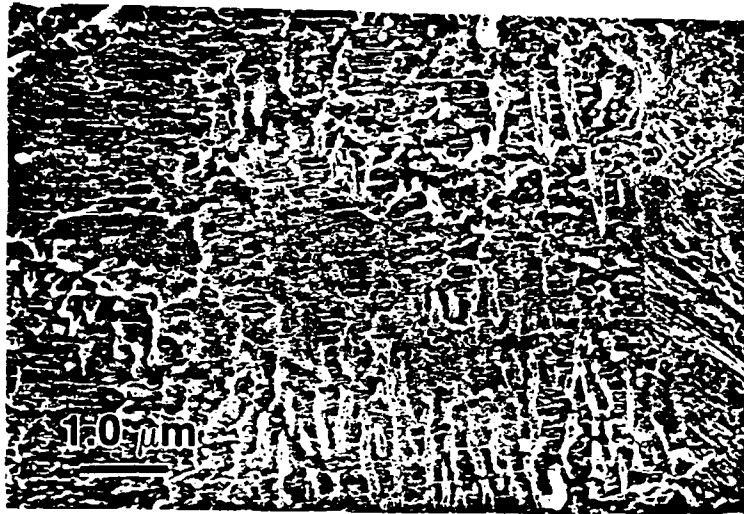
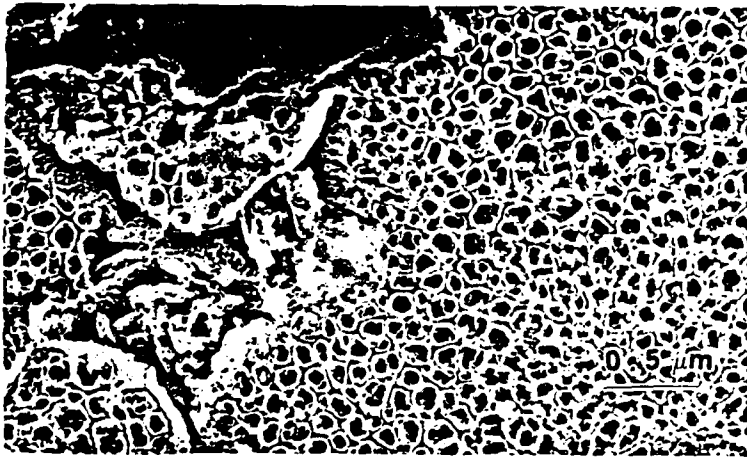


Figure 26: STEM photomicrographs of Ti-6-4 surface etched by the phosphate fluoride treatment.

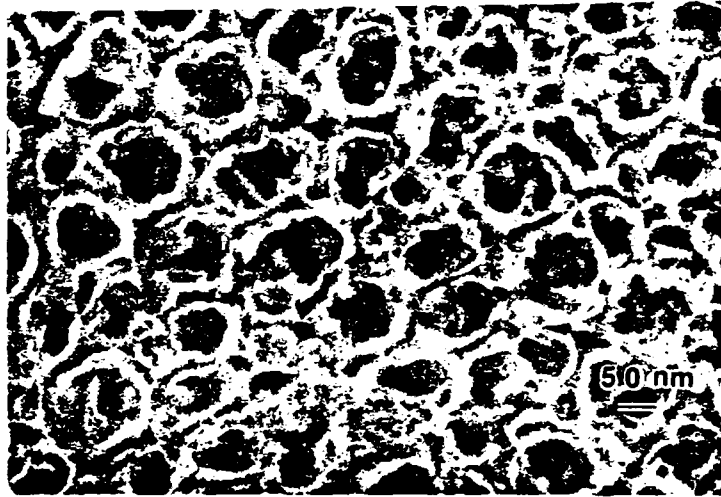


a



b

Figure 27: STEM photomicrographs of CAA Ti-6-4 at 10 V with current density adjust by HF ($i=5.47 \text{ mA/cm}^2$), at 54 degree C for 20 minutes. (a) 4,300X (b) 25,000X.



a

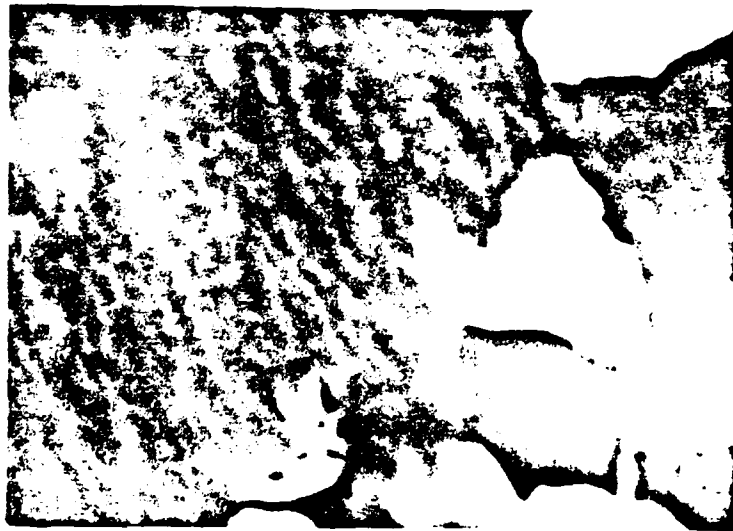


b

Figure 28: STEM photomicrographs of CAA Ti-6-4 at 10 V for 20 minutes at 54 degree C with $I=5.47 \text{ mA/cm}^2$ adjusted by HF addition. (a) 100,000X (b) 100,000X.



a

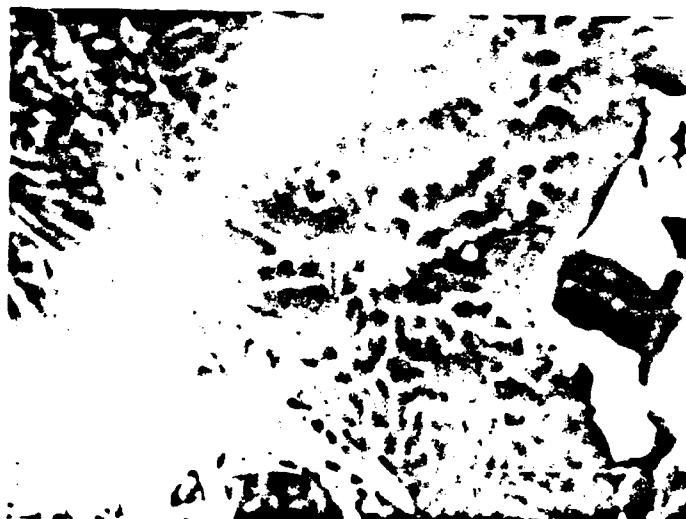


b

Figure 29: SEM photomicrographs of CAA Ti-6-4 at 9 W for 30 minutes. (a) with HF addition (b) without HF. (18 000x)

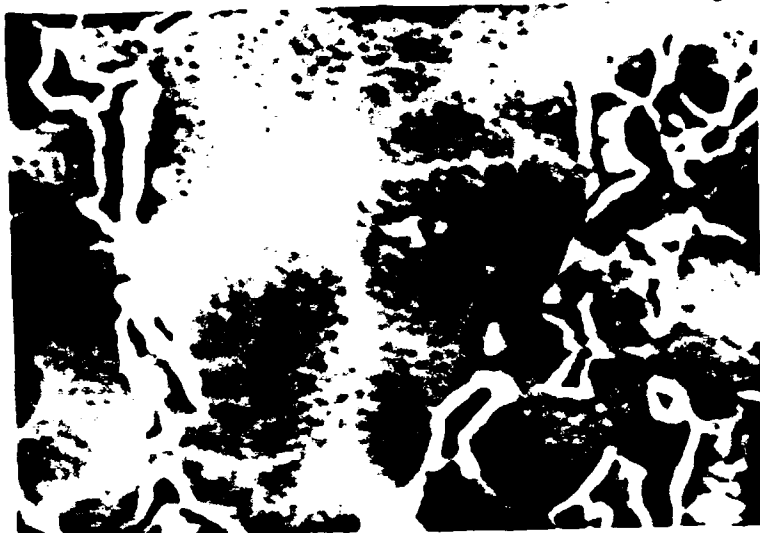


a



b

Figure 30: SEM photomicrographs of CAA Ti-6-4 at 9 V for 20 minutes. (a) with HF addition (b) without HF. (18,000X)

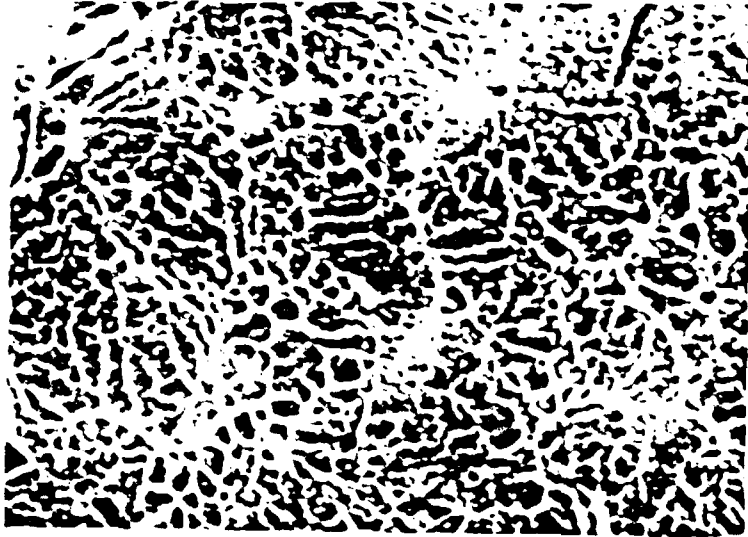


a



b

Figure 31: SEM photomicrographs of CAA Ti-6-4 at 10 V for 20 minutes. (a) with HF addition (b) without HF. (10,000X)



a



b

Figure 32: SEM photomicrographs of CAA Ti-6-4 at 10 V for 16 minutes. (a) with HF addition. (b) Without HF (10,000X)

interference color, which was visible within seconds after the coupon was polarized, remained unchanged throughout the experiment. When HF was used, the interference color changed with time of anodization at a constant voltage. For example, when anodized at 10 V, a brilliant light blue color was obtained if no HF was present. The same blue color changed to light yellow, light brown, purplish red and purplish blue at 7 min., 11 min., 16 min. and 20 min., respectively, when HF was added. This infers that the thickness of the oxide was changing with anodizing time. It is likely that HF enhances the uniform dissolution of the oxide in chromic acid and leads to oxide thinning with time until equilibrium is reached.

5.5 X-RAY PHOTOELECTRON SPECTROSCOPY

X-ray photoelectron spectroscopy (XPS OR ESCA) is a widely used surface analysis tool. Elemental and chemical bonding information can be derived from the photoelectron peaks. XPS is very surface sensitive; only the top 10 nm or less are examined. Since only soft X-rays are used to probe the sample surface, it can be applied to polymeric materials as well as metals. The principles and applications of XPS for surface analysis have been published in a number of books[90-92] and, therefore, will not be discussed

A typical (sample B in Table 4) XPS spectrum for an anodized Ti-6-4 sample is shown in Figure 33. The major photoelectron and Auger peaks were as identified.

The Ti 2p doublet at 458.9 eV and 464.6 eV suggested that the Ti on the surface was in an oxidized form. The 5.7 eV separation between the doublet was indicative that the Ti was in the form of TiO_2 [93].

The curve-fitted oxygen 1s peak showed that there were three component peaks. The peak at 530.4 eV represents the oxygen bonded to Ti as in TiO_2 . The peak at 531.2 eV is probably due to oxygen in the hydroxide or H_2O form while the peak at 533.0 eV is probably from contamination during sample handling.

The carbon peak was due to hydrocarbon contamination on the sample. This carbon peak was used as a reference to determine the peak shift as a result of sample charging and work function of the spectrometer. Table 4 shows the elements identified on selected samples. The major peaks which were common to all samples were the oxygen, titanium and carbon as expected. Only trace amount of aluminium and no vanadium was detected. The absence of vanadium on the surface again suggests that the beta phase alloy was preferentially etched out either during the acid pickling or in the anodizing bath. Although it was expected that

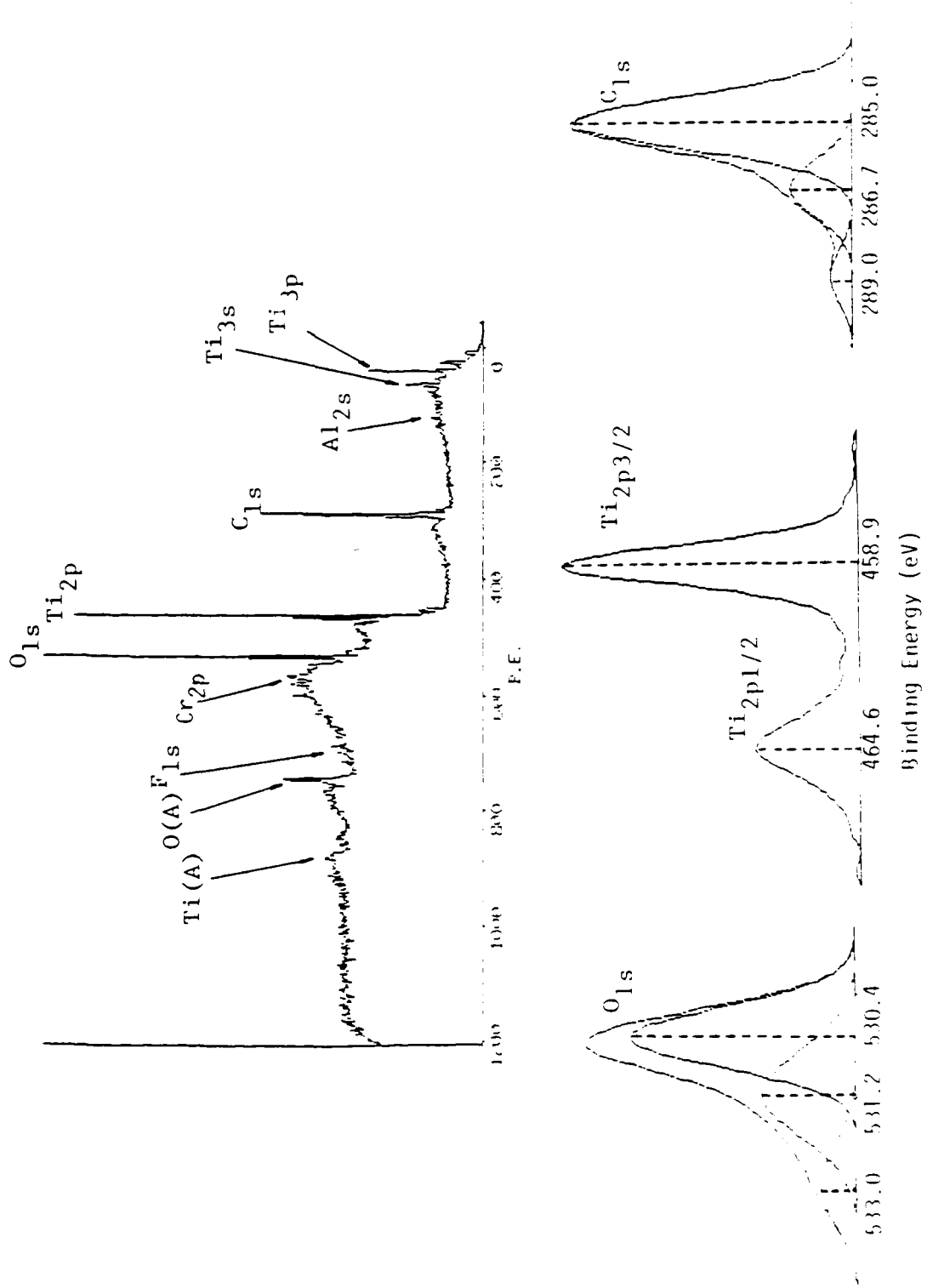
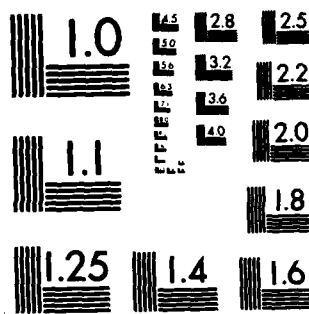


Figure 33: Wide and narrow scans XPS spectra of CAA Ti-6-4 surface.



MICROCOPY RESOLUTION TEST CHART
NATIONAL BUREAU OF STANDARDS-1963-A

chromium would be present because of the chromic acid used in the anodization, chromium was not detected in any significant amount. It is worth pointing out, however, that samples anodized with addition of HF showed fluorine on the surface.

TABLE 4

XPS peak position of elements on CAA Ti-6-4 surfaces

PHOTOELECTRON	SAMPLES				
	A	B	C	D	E
PEAKS	_____	_____	_____	_____	_____
	Binding Energy (eV)				
C _{1s}	285.0	285.0	285.0	285.0	285.0
O _{1s}	530.1	530.1	530.1	530.3	529.8
Ti _{2p3/2}	458.7	458.9	458.9	458.9	458.3
F _{1s}	-----	684.8	-----	-----	-----
Cr _{2p}	-----	-----	-----	-----	-----
Al _{2s}	-----	-----	-----	-----	-----
V ₂	-----	-----	-----	-----	-----

----- not detectable or less than 1%.

- A. CAA at constant CD= 2.15 mA/cm² and switched to constant 10 V when voltage peaked.
- B. CAA at constant 10 V with HF addition.
- C. CAA at constant CD= 2.15 mA/cm².
- D. CAA at constant CD= 2.65 mA/cm².
- E. CAA at constant CD= 11.59 mA/cm² at which oxide breakdown occurred.

Chapter VI

SUMMARY

The galvanostatic experiments indicated that the anodic film formation on Ti-6-4 in chromic acid can be described by a simple model. The data showed reasonably good agreement with calculations based on a compact, pore-free film with 100% current efficiency. STEM and SEM micrographs showed that the film formed was indeed a smooth, compact film.

A distinct transition occurs at current density around 10^{-4} A/cm². This was probably due to some changes in the nature of the film in response to the change in current density.

The electrolyte parameters A and B are characteristic of the anodizing system. The parameter A is a measure of the potential energy barrier for ion migration and is proportional to pH while B is proportional to the activation distance "a", which is half the distance the ion advances in each lattice jump. It was found that an oxide layer in the order of 10 Angstrom was present on the metal surface before anodization. The thickness of this pre-immersion oxide is expected to vary depending on the sample preparation technique used. In any case, the samples should be pickled to remove the existing oxide, rinsed in distilled water and

transferred to the anodizing bath as soon as possible to minimize oxidation in air and water.

From the STEM and SEM micrographs obtained during potentiostatic anodization, it can be concluded that no porosity exists on the oxide formed in 20 minutes or less. This is expected (from figure 21) because at 20 minutes, the film is basically still the original insulating barrier layer allowing minimum current flow. However, in the presence of HF, micro-porosity was observed regardless of the voltage, time and temperature. It is important to point out that at higher temperature and more HF, the pore size became larger. This seems to support the idea that pore initiation is a dissolution process activated by HF and enhanced by high temperature. Dissolution was also evident from the change in interference color of the coupon during anodization with HF. HF probably promotes uniform thinning as well as localized attack on the oxide resulting in thinning at specific sites. Current concentrates on the thin spots leading to Joule heating and faster dissolution at the pore base until equilibrium is established.

Results from XPS indicated that the oxide on the anodized surface is indeed TiO_2 . Apart from the hydrocarbon contaminations, no other major element was present. Trace amount of chromium was found as residual from the chromic

acid. HF was identified on surfaces anodized with HF addition. The effects of fluorine contamination on bonding is not clear at this point. Further studies are needed to determine whether it has similar deleterious effects on Ti-6-4 as in aluminum.

REFERENCE

1. W.T. Highberger, 12th National SAMPE Tech. Conf., Oct 7-9(1980).
2. P.H. Morton, Rosenhain Centenary Conf., Phil. Tran. of the Royal Society, 282A,1307(1975).
3. M.J. Hiler, Adhesive Age, Jan(1967).
4. J.J. Bikerman, "Science of Adhesive Joints," Interscience, 1968.
5. B.M. Vanderbilt and R.E. Clayton, Ind. Eng. Chem., 4, 18(1965).
6. M.C. Polniazek and R.M. Schaufelberger, Adhesive Age, 11(7), 25(1968).
7. P. Walker, J. Coatings Technol. 52, 670(1980).
8. A.J. Kinlock, et.al., "Adhesion Science and Technology," New York, 1975.
9. N.J. DeLollis, Adhesive Age, 21, Dec.(1968).
10. W.K. Zisman, Adv. Chem. Ser., 43, 1(1964).
11. M. Brenman and CH.H. Lerchenthal, Poly. Eng. Sci., 16, 747(1976).
12. CH.H Lerchenthal and M. Brenman, Poly. Eng. Sci., 16, 760(1976).
13. S.S. Voyutskii, "Autohesion and Adhesion of High Polymers," Interscience, New York, 1963.
14. B.V. Derjaguin, N.A. Krotova and V.P. Smilga, "Adhesion of Solids," translated by R.K. Johnston, Consultants Bureau, New York, 1978.
15. S.M. Skinner, R.L. Savage, and J.E. Rutzler Jr., J. Appl. Phys., 24, 438(1953).
16. S.M. Skinner, J. Appl. Phys., 26, 498(1955).

17. F.M. Fowkes, in " Polymer Science and Technology," Vol. 12A, L-H Lee, Ed., Plenum Press, New York, 1979.
18. M.J. Marmo, M.A. Mostafa, H. Jinnai, F.M. Fowkes and J.A. Manson, Ind. Eng. Chem. Prod. Res. Dev., 15, 206(1976).
19. F.M. Fowkes, C-Y Sun and S.T. Joslin, in " Corrosion Control by Organic Coatings," H. Leidheiser, Jr., Ed., NACE, 1981.
20. J.G. Mason, R. Siriwardane and J.P. Wightman, J. Adhesion, 11, 315(1981)
21. K. Bright, B.W. Malpass and D. E. Packham, Nature, 223, 1360(1969).
22. D.E. Packham, K. Bright and B.W. Malpass, J. Apply. Polym. Sci., 18, 3237(1974).
23. B.W. Malpass, D.E. Packham and K. Bright, J. Appl. Polym. Sci., 18, 3249(1974).
24. D.J. Arrowsmith, Trans. Inst. Met. Finish., 48, 88(1970).
25. A.F. Lewis and R.T. Natarajan, in "Polymer Science and Technology," Vol. 9A, L-H Lee, Ed., Plenum Press, New York, 1975.
26. W.L. Baun, J. Adhesion, 12, 81(1981).
27. F.A. Cotton and G. Wilkinson, "Advanced Inorganic Chemistry," 4th ed., Interscience, 1980.
28. M. Pourbaix, "Lectures on Electrochemical Corrosion," Plenum Press, New York, 1973.
29. T.P. Hoar, in "Modern Aspects of Electrochemistry," No.2, J.O'M Bockris, Ed., Butterworths Scientific, London, 1959.
30. J.P. Frayret and A. Caprani, Electrochim Acta, 26(12), 1789(1981); 27(3), 391(1982).
31. T. Hepel, M. Hepel and R. Osteryoung, J. Electrochem. Soc., 129, 2132(1982).
32. P.J. Boddy, J. Electrochem. Soc., 115, 199(1968)

33. A. Guntherschulze and H. Betz, *Z. Phys.*, 68, 145(1931); 92, 367(1934).
34. E.J.W. Verwey, *Physica*, 2, 1059(1953).
35. N.F. Mott, *Trans. Faraday Soc.*, 43, 429(1947).
36. N. Cabrera and N.F. Mott, *Repts. Prog. Physics*, 12, 163(1948-9).
37. D.A. Vermilyea, *Acta Met.*, 1, 282(1953).
38. J.F. Dewald, *J. Electrochem. Soc.*, 102, 1(1955).
39. C.D. Hall, Jr., and N. Hackerman, *J. Phys. Chem.*, 57, 262(1953).
40. H.A. Johansen, G.B. Adams and P. Van Rysselberghe, *J. Electrochem. Soc.*, 104, 339(1957).
41. M.E. Sibert, *J. Electrochem. Soc.*, 110, 65(1963).
42. J. Green and A. Sedricks, *Met. Trans.*, 2(7), 1807(1971).
43. G. Hass, *Vacuum*, 11, 331(1952).
44. F. Cover and M. Musselin, *Thin Solid Films*, 2(3), 211(1968).
45. S. Khoo, G. Wood and D. Whittle, *Electrochim. Acta*, 16, 1703(1971).
46. I.A. Ammar and I. Kamal, *Electrochim. Acta.*, 16, 1539(1971).
47. A. Aladjem, M. Aucouturier and P. Lacombe, *J. Mater. Sci.*, 8, (973).
48. M. Stern, *J. Electrochem. Soc.*, 105, 11(1958).
49. J.E. Lewis and R.C. Plumb, *J. Electrochem. Soc.*, 105, 496(1958).
50. D.A. Vermilyea, *Acta Met.*, 2, 482(1954).
51. J.J. Randall, W.J. Bernard and R.R. Wilkinson, *Electrochim. Acta*, 10, 183(1965).

52. J.A. Davies, J.P.S. Pringle, R.L. Graham, and F. Brown, *J. Electrochem. Soc.*, 109, 999(1962).
53. J.A. Davies and B Domeij, *J. Electrochem. Soc.*, 110, 84(1963).
54. J.A. Davies, B Domeij, J.P.S. Pringle, and F. Brown, *J. Electrochem. Soc.*, 112, 675(1965).
55. D.A. Vermilyea, *J. Electrochem. Soc.*, 110, 345(1963).
56. D.A. Vermilyea, *J. Electrochem. Soc.*, 110, 250(1963).
57. A.T. Fromhold, Jr., *Surf. Sci.*, 22, 396(1970).
58. N. Sato, *Electrochim. Acta*, 16, 1683(1971).
59. T.P. Hoar, *Corros. Sci.*, 7, 341(1967).
60. A.R. Piggott, H. Leckie and L.L. Shreir, *Corros. Sci.*, 5, 165(1965).
61. J. Yahalom and J. Zahavi, *Electrochim. Acta*, 15, 1429(1970).
62. D. Dobos, "Electrochemical Data," Elsevier Scientific, New York, 1975.
63. D.A. Vermilyea, *J. Electrochem. Soc.*, 104, 485(1957).
64. B.M. Ditchek, K.R. Breen, T.S. Sun, J.D. Venables and S.R. Brown, *Proc. 12th Nat. SAMPE Tech. Conf.*, Oct.7-9 (1980).
65. W.L. Baun, *Surf. Technl.*, 11, 421(1980).
66. J.D. Venables, D.K. McNamara, J.M. Chen, T.S. Sun and R.L. Hopping, *Appl. Surf. Sci.*, 3, 88(1979).
67. G.C. Wood, in "Oxides and Oxide Films," Vol.2, J.W. Diggle, Ed., Marcel Dekker, Inc., New York, 1973.
68. T.P. Hoar and J Yahalom, *J. Electrochem. Soc.*, 110, 614(1963).
69. J.P. O'Sullivan and G.C. Wood, *Proc. Roy. Soc.*, A317, 511(1970).

70. M. Pourbaix, "Atlas of Electrochemical Equilibria in Aqueous Solutions," Pergamon Press, London, 1966.
71. S. Yamaguchi, J. Electrochem Soc., 108, 302(1961).
72. A.C. Fraker and A.W. Ruff, Jr., Corros. Sci., 11, 763(1971).
73. T. Koizumi and T. Nakayama, Corros. Sci., 8, 195(1968).
74. K.W. Allen and H.S. Alsalim, J. Adhesion, 6, 229(1974).
75. M. Natan and J.D. Venables, J. Adhesion, 15, 125(1983).
76. J.D. Briers, Optik, 63, 341(1983).
77. A.H. Musa and W.E.J. Neal, Surf. Technl., 11, 323(1980).
78. G. Hass and A.P.J. Bradford, J. Opt. Soc. Am., 47, 125(1975).
79. J.J. Carroll and A.J. Melmed, J. Opt. Soc. Am., 64, 514(1974).
80. T. Smith, J. Opt. Soc. Am., 62, 774(1972).
81. C.R. Menard, J. Opt. Soc. Am., 52, 427(1962).
82. R.H. Shoemaker, in "Titanium Science," Vol. 4, Plenum Press, New York, 1973.
83. L.H. Sharpe, J. Adhesion, 4, 51(1972).
84. J. Yahalom and T.P. Hoar, Electrochim. Acta, 15, 877(1970).
85. S. Darwish, Corrosion, 27, 265(1971).
86. G.V. Samsonov, Ed., "The Oxide Handbook", Plenum, New York, 1981.
87. Y. Moji and J.A. Marceau, U. S. Patent 3,959,091, May 25, 1976.

88. O.T. Sørensen, Ed., "Nonstoichiometric Oxides," Academic Press, New York, 1981.
89. A.T. Fromhold, Jr., in "Oxides and Oxide Films," Vol. 3, J.W. Diggle and A.K. Vijh, Ed., Marcel Dekker, Inc., New York, 1976.
90. D.W. Dwight, T.J. Fabish and H.R. Thomas, Ed., "Photon, Electron, and Ion Probes of Polymer Structure and Properties," ACS Symposium Series 162, ACS, Washington, D.C., 1981.
91. P.K. Ghosh, "Introduction to Photoelectron Spectroscopy," Interscience, New York, 1983.
92. D. Briggs, Ed., "Handbook of X-ray and Ultraviolet Photoelectron Spectroscopy," Heyden, Philadelphia, 1977.
93. C.D. Wagner, W.M. Riggs, L.E. Davis, J.F. Moulder and G.E. Muilenberg, Ed., "Handbook of X-ray Photoelectron Spectroscopy," Perkin-Elmer Corp., Minnesota, 1979.

Appendix A

A.1 CALCULATION OF FORMATION RATE AND ELECTROLYTIC PARAMETERS

The assumed model of the anodic oxide system is shown in Fig. 34. If film is uniform and compact with 100% current efficiency, the equation describing the change in film thickness with applied charge is,

$$\Delta\delta = (M/\rho\sigma nF)\Delta Q \quad (7)$$

where δ = total film thickness, M = molecular weight of the oxide, σ = roughness factor, n = number of Faradays involved per mole of oxide formed, F = Faraday constant (96487 C/mole) ρ = density of the oxide and Q = charge density.

Let $r = (M/\rho nF)$ and, assuming constant current density, $\Delta Q = I\Delta t$.

Then,

$$\Delta\delta = (rI\Delta t/\sigma) \quad (8)$$

Since, $\delta = \delta_0 + \Delta\delta$

Therefore, $\delta = \delta_0 + (rIt/\sigma) \quad (9)$

where δ_0 = pre-immersion oxide thickness.

From the work of Guntherschulze and Betz[33],

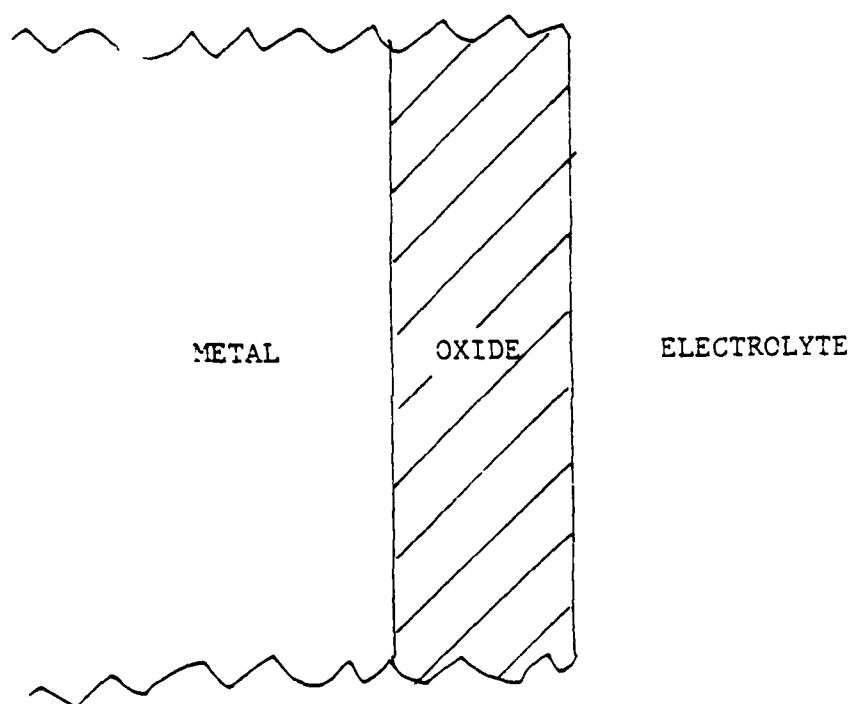


Figure 34: Model of metal/oxide system

$$I = A \exp(BH) \quad (1)$$

where I = current density, H = field strength, and A and B are electrolytic parameters.

The total potential drop in the circuit is,

$$E = E_f + \phi \quad (10)$$

E_f = potential drop across the film

ϕ = Potential drop due to other resistance in the system

By definition the field strength is: $H = E_f/\delta \quad (11)$

Now, from equations (1), (9) and (11)

$$I = A \exp(B E_f/\delta) \quad (12)$$

and, $I = A \exp(B E_f/(\delta_0 + rIt/\sigma)) \quad (13)$

Rearranging equation (13) gives

$$E_f = (\delta_0/B + rIt/B\sigma) \ln(I/A) \quad (14)$$

From equations (10) and (14), it follows that

$$E = \phi + (\delta_0/B) \ln(I/A) + (rIt/B\sigma) \ln(I/A) \quad (15)$$

Taking the derivative of equation (15) WRT time, t ,
at constant I yields:

$$(dE/dt)_I = (rI/B\sigma)\ln(I/A) \quad (16)$$

From equation (16), we can see that the slope of the E vs. t curve at constant I should be constant.

Dividing both sides of equation (16) by I yields:

$$(dE/Idt)_I = (r/B\sigma)\ln(I/A) \quad (17)$$

with $dQ = Idt$, equation (17) gives:

$$(dE/dQ)_I = (r/B\sigma)\ln(I/A) \quad (18)$$

$(dE/dQ)_I$ is known as reciprocal capacitance ($1/C$) or unitary formation rate (R_i) which is constant for constant I.

$$(dE/dQ)_I = 1/C = R_i = (r/\sigma B)\ln(I/A) \quad (19)$$

The plot of $(dE/dQ)_I$ vs. $\ln I$ will give a straight line with slope of $(r/\sigma B)$ and intercept of $(r \ln A/\sigma B)$. From this plot, the electrolytic parameters A and B can be evaluated.

Rearranging equation (1) gives, $H = (1/B) \ln(I/A)$

Since $(1/C) = (r/\sigma B) \ln(I/A)$, from equation (19),

$$\text{now, } H = (\sigma/r)(1/C) \quad (20)$$

Taking the derivative of equation (15) WRT $\ln I$ at constant t yields:

$$\frac{dE}{d\ln I}_t = \delta_o/B + I(rt/B\sigma)\{1 + \ln(I/A)\} \quad (21)$$

From (21), $(dE/d\ln I)_t$ is a function of I . Therefore, the plot of $(dE/d\ln I)_t$ vs. $\ln I$ would give a curve with slope increasing with increasing I .

Substituting $Q=It$ into equation (15) gives,

$$E = \delta + (\delta_o/B)\ln(I/A) + (rQ/B\sigma)\ln(I/A) \quad (22)$$

Taking the derivative of (22) WRT $\ln I$ at constant Q gives,

$$\frac{dE}{d\ln I}_Q = (\delta_o/B + rQ/B\sigma) \quad (23)$$

equation (23) shows that the plot of E vs. $\ln I$ at constant Q will give a straight line since all the quantities on the right of equation (23) are constants.

The pre-oxidation thickness can be calculated by rearranging equation (23) yielding:

$$\delta_o = B(dE/\ln I)_Q - (rQ/\sigma) \quad (25)$$

REPORT DOCUMENTATION PAGE		READ INSTRUCTIONS BEFORE COMPLETING FORM
1. REPORT NUMBER	2. GOVT ACCESSION NO. AD-A240057	3. RECIPIENT'S CATALOG NUMBER
4. TITLE (and Subtitle) Anodic Oxide Formation on Ti-6Al-4V in Chromic Acid for Adhesive Bonding		5. TYPE OF REPORT & PERIOD COVERED Interim, 9/30/82-12/30/83
		6. PERFORMING ORG. REPORT NUMBER
7. AUTHOR(s) Alvin Man-tuen Cheng and David W. Dwight		8. CONTRACT OR GRANT NUMBER(s) ONR N00014-82-K-0185
9. PERFORMING ORGANIZATION NAME AND ADDRESS Center for Adhesion Science and Departments of Chemical Engineering and Materials Engineering, VPI & SU, Blacksburg, VA 24061		10. PROGRAM ELEMENT, PROJECT, TASK AREA & WORK UNIT NUMBERS
11. CONTROLLING OFFICE NAME AND ADDRESS Office of Naval Research 800 N. Quincy St. Arlington, VA 22217		12. REPORT DATE March 1984
		13. NUMBER OF PAGES
14. MONITORING AGENCY NAME & ADDRESS (if different from Controlling Office)		15. SECURITY CLASS. (of this report)
		15a. DECLASSIFICATION/DOWNGRADING SCHEDULE
16. DISTRIBUTION STATEMENT (of this Report) Distribution Unlimited		
17. DISTRIBUTION STATEMENT (of the abstract entered in Block 20, if different from Report)		
18. SUPPLEMENTARY NOTES		
19. KEY WORDS (Continue on reverse side if necessary and identify by block number) Anodization; Titanium Alloy; Ti 6-4; Ti 6Al-4V; Adhesive Bonding, Surface Treatment; Porous Oxide; STEM; SEM; ESCA; XPS		
20. ABSTRACT (Continue on reverse side if necessary and identify by block number) Chromic acid anodization (CAA) of Ti-6Al-4V alloy has been shown to produce desirable oxide for adhesive bonding. The highly porous oxide layer provides mechanical interlocking with the adhesive or the primer forming a much stronger interface. This leads to stronger and more durable bonds than most other surface pretreatments. Since anodization is an electrochemical process, electrochemical methods are used to elucidate the mechanism and kinetics of the oxide formation. From galvanostatic anodization, the preimmersion oxide thickness is calculated to be in the order of 10 Angstrom. Oxygen evolution is dominant at above 10 V. Oxide (over		

(Block 20 continued)

breakdown or cracking was observed at potentials above 10 V and at current density above 11 mA/cm². Hydrofluoric acid was found to be essential in the initiation and formation of pores desirable for adhesive bonding. Without HF addition, the oxide formed was compact and uniform regardless of anodizing conditions (before breakdown). In the presence of HF, porous oxide was obtained with pore size distribution increasing with temperature and HF concentration.

LMED
— 8

